NUST JOURNAL OF ENGINEERING SCIENCES

Vol. 18, No. 1
June 2025
ISSN 2070-9900
E-ISSN 2411-6319

Subscriptions		
Inland	Annual	Per copy
• Institutions	Rs. 1000.00	Rs. 400.00
• Individuals	Rs. 800.00	Rs. 300.00
• Students	Rs. 600.00	Rs. 250.00
Overseas		
• Institutions	US $ 250.00	US $ 100.00
• Individuals	US $ 200.00	US $ 80.00
• Students	US $ 150.00	US $ 60.00

Note:

- Subscription rates include postage inland and overseas.
- All requests/subscriptions/queries should be addressed to Editor, NJES, National University of Sciences & Technlology, H-12, Islamabad 44000, Pakistan.
- Bank drafts/pay orders should be in favour of NUST.

Printed By: NUST University Press
Phone: +92-51-9085-1381
Email: prnust@gmail.com
Website: www.nust.edu.pk

Postal Address:
National University of Sciences & Technology
Sector H-12, Islamabad, Pakistan.

Aims and Scope

The NUST Journal of Engineering Sciences (NJES) Publishes original contributions on all aspects of engineering sciences. The Journal is originally intended to serve as a platform for publication of international quality peer-reviewed research work in the relevant field. Submission of the manuscript implies that it is not being simultaneously considered for publicationelsewhere and that the authors have obtained the necessary authority for publication. NJES aims to provide a rapid channel for the publication of full-length papers on engineering sciences. For the sake of efficient communication, authors are requested to formulate their results in a concise and compactform. Each paper should be self-contained, properly introduced, with references to published work, and fully documented with adequate source materials.

Publication Policy and Instruction for Preparation of Manuscripts

General Requirements

The title page should contain (1) Title of the article (not more than 200 characters), center justified, bold, "Times New Roman, 14 point" (2) Name(s) of the Author(s) (not more than 10), information about the corresponding author, affiliation(s), addresses, center justified "Times New Roman, 12 point" (3) Abstract, keywords 5 to 10, (4) Start of the main text, justified, "Times New Roman, 12 point". The rest of the pages would contain the main text, Acknowledgements (if applicable), Appendices, References, Figures with captions, Tables with captions, justified, "Times New Roman, 12 point". All headings should be flushed with left margin, "Times New Roman, 12 point, bold". Editors reserve the right to adjust style to ensure standards of uniformity. All texts should be submitted in Microsoft Word; no other format is acceptable.

Corresponding/Main author

Please indicate clearly who is willing to handle correspondence at all stages of refereeing, publication and post-publication. Please ensure that telephone and fax numbers are provided in addition to e-mail and postal address. Full postal addresses must be given for all co-authors.

Abstract

The abstract should consist of about 250 words, describing background, objectives, methods and results. The format of abstract is described under general requirements.

Introduction

Under this heading, please state the purpose of the article and summarize the rationale for the study. Please provide the relevant references only; do not include data or conclusions in this section.

Methods

Identify the method of investigation, relevance and equipment used, with information about the model and

manufacturer. Please also provide reference to the earlier work and enough details to allow subsequent investigations on the subject. Please do specify each starting material, chemicals, raw material, chemical equations, process and scientific justifications.

Results and discussion

The results should be presented in a logical sequence. Tables and figures should be numbered and inserted close to the point of discussion. The captions for tables should be sequentially numbered and placed at the top of the table, whereas the same should be placed below the figure. During the discussion, please emphasize new aspects of the study and the conclusions that follow from them. Link the conclusions with the goals of the study provided in the introduction. Please avoid statements that are not substantiated experimentally. Confirmistic statements should also be avoided unless supported by overwhelming experimental evidence. New hypotheses may be stated when warranted but used in association with appropriate recommendations.

Acknowledgments

Those persons or organizations may be acknowledged who contributed physically or intellectually to the research. Technical help does not justify the authorship of the paper. It maybe acknowledged in a separate paragraph.

References

References should be listed at the end of the paper in the order in which they occur in the text. Cross references may be made within the text in case required. They should be indicated within the text by square bracket [2]. Examples:

Books: F. G. Hodge., "Nickel and high nickel alloys", P. A. Schweitzer, ed., Corrosion and Corrosion Protection handbook, New York: Marcel Dekker, 1983, pp. 75-6.

Dissertations/theses: R. J. King, "Corrosion of steel weldments in permafrost", Ph.D. Thesis, The University of Calgary, Calgary, Canada, 1983.

Periodicals: N. A. Shah, A. Ali and A. Maqsood, "Preparation and characterization of CdTe for solar cells, detectors and related thin film materials", Journal of Electronic Materials, Vol. 37, No. 2, 2008, pp. 145-151.

Conference proceedings: C. Feng "Transformation and structural changes in metals under shock and dynamic loading", Proceedings of International Conference on High Strain-Rate Phenomena in Materials, San Diego, CA, August 12-16, 1990.

Technical reports: E.E. Reber, R. L. Mitchell and C. J. Carter, "Oxygen absorption in the earth's atmosphere", Aerospace Corp., Los Angeles, CA, Tech. Rep. Tr-0200 (4230-46)-3, Nov. 1968.

Websites: B. Brandstaetter, "SMES optimization benchmark, TEAM problem 22, 3 parameter problem", http://www.igte.tu - graz.ac.at/archive/team _new/team3.php. September 10, 2008.

Figures and tables

Figures and tables should be typed as part of the text and must be separated from the text by a two-line space above and below the table in Microsoft Word. Please use the table option to create tables. The table should be inserted in the text close to the point of reference, and the author(s) must make sure that a table does not run over to the next page. The captions for tables should be numbered sequentially and placed at the top of the table, whereas the same should be placed below the figure. Please ensure that figures/tables are legible in 3.2" column space.

Abbreviations and footnotes

Abbreviations should be defined when first used in text but should not be used in the abstract. Abbreviations for instruments (e.g., SEM and TEM should not be used for methodologies such as scanning electron microscopy and transmission electron microscopy). Footnotes may be added at the discretion of the authors where additional definition, explanation, or acknowledgment is deemed necessary. Manufacturer citations of trade names, instruments, model numbers, and products unique to the study may be included in the text. Footnotes will not be included in the reference list.

Units

Authors are encouraged to adhere to the basic SI system of units. If the use of SI units would hinder reader comprehension, then alternate metric units may be used. All data should then be given in metric units with a list of conversion factors used.

Submission of manuscript

The manuscript should be submitted electronically via online submission at

https://journals.nust.edu.pk/index.php/njes/index

NUST JOURNAL OF ENGINEERING SCIENCES

NUST JOURNAL OF ENGINEERING SCIENCES

Contents

Disrupting HBV Persistence: Genetic Engineering Approach to Break the Oncogenic HBx Gene

Saleha Resham, Haiqa Khan, Fazal Adnan*, Sobia Manzoor
Atta ur Rahman School of Applied Biosciences, National University of Science and Technology (NUST)
*Corresponding author: adnanfazal@asab.nust.edu.pk
Received: 21-04-2025, Received in Revised form: 08-05-2025, Accepted: 30-06-2023, Published: 30-06-2025

Abstract

Chronic Hepatitis B virus (HBV) infection can cause liver cirrhosis or cancer, making it a persistent worldwide health concern. Nucleoside analogs used in current antiviral treatments can prevent HBV from replicating, but they do not break the covalently closed circular DNA that HBV currently possesses. This study presents the state-of-art-technology as an alternative treatment option to control the disease. Using the program CRISPR RGEN (http://www.rgenome.net/) the gRNAs were designed and cloned insilco in mammalian expression (vector px260, Addgene) and were later sent for commercial synthesis to be synthesized and cloned in the px260 vector. Propagated in E. coli DH5 alpha cells, the custom cloned vector construct was isolated and visualized using gel electrophoresis. Cell culture-based testing performed at the Hepatitis Laboratory (University Airrlanga Indonesia). Huhit cells were utilized for lipofectamine mediated transfection. However, after successful transfection, confirmation was done through PCR and Sanger sequencing. An efficient plasmid based CRISPR/CAS9 vector has been designed and constructed successfully to target HBx gene in liver cells. Plasmid´s, cloning propagation, isolation and confirmation were done in bacterial cells (selected through antibiotic). The initial phase of testing on Huhit cells was performed. However further validation experiments on HepG2 cells and mice models are the prospects based on positive outcome of previous testing. The goal of this planned study is to use CRISPR/cas9 genome editing technology therapeutically targeting oncogenic Hbx gene of HBV.Which could speed up the development of anti-HBV CRISPR/Cas 9 based therapies in conjunction with currently available treatments (NAs).

Keywords: CRISPR/Cas9, HBV, HBX, IFN, Anti-HB.

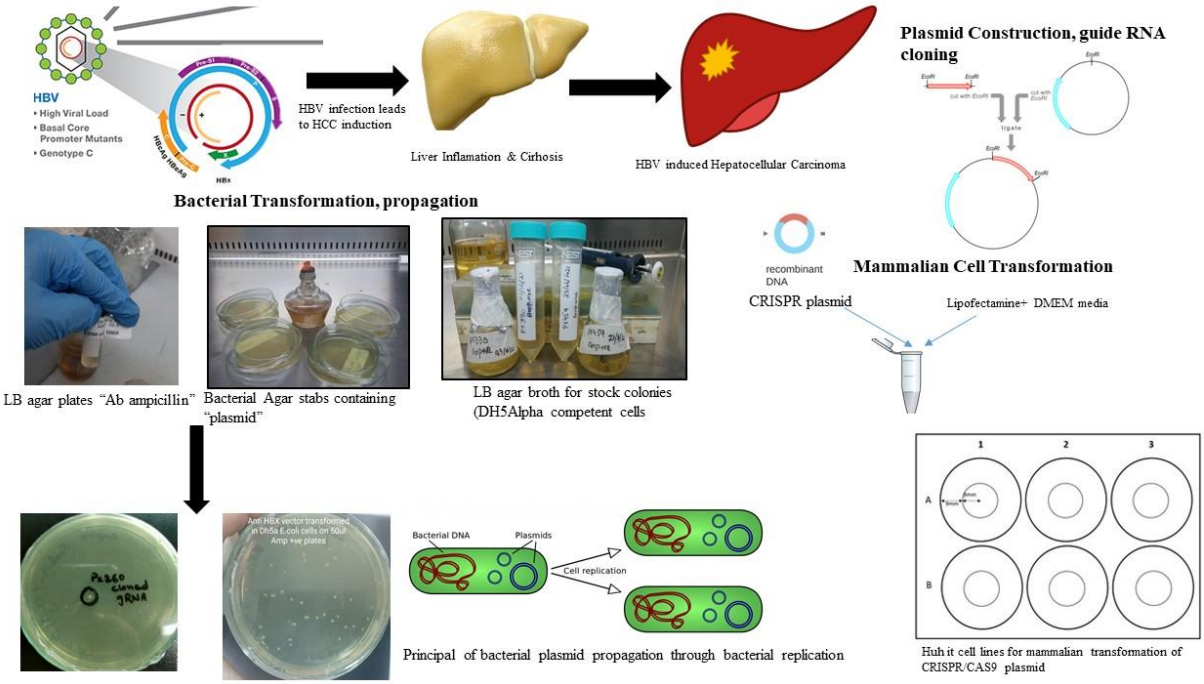

Graphical Abstract

Introduction

Across the world, the leading cause of liver disease is chronic HBV infection. In the World Health Organization's 2018 report on worldwide cancer statistics, liver cancer ranked sixth worldwide and is the fourth-leading cause of cancer-related fatalities[1]. Despite the development of effective vaccines, HBV infection is still a major issue of global public health. A recent survey estimated that 240 million persons are chronically infected by HBV, a sizable portion of whom require antiviral therapy to prevent the long-term detrimental consequences, including cirrhosis and HCC [2, 3]. Currently, two types of antiviral therapy, interferon-alpha (IFN- α) and nucleos(t)ide analogue (NA), are available for chronic hepatitis B (CHB) [3]. IFN acts through both direct antiviral and indirect immunomodulatory effects, while NA suppresses viral replication by inhibiting the viral polymerase. Although effective, neither of them has satisfactory sustained off-therapy responses. Most patients suffer from rebound viremia and relapsing hepatitis after the cessation of antiviral therapy and often must receive life-long treatment. Long-term antiviral therapy not only has a potential risk for the emergence of drug resistance but also imposes a high socio-economic burden in HBV endemic countries. As a result, a novel therapy for curing chronic HBV infection is still in pressing need.[4]

Methodology

In-silico guide RNA Design

https://doi.org/10.24949/njes.v18i1.905
This work was presented at 4th ASEAN Pakistan Conference on Materials Science (APCOMS), 2025.

An online webtool CRISPR RGEN (http://www.rgenome.net/) was used to design gRNAs against *HBV X* gene (HBV ayw strain). Table 1 shown below gives the sequence of 2 guide RNA sequences, designed and used in the study, along with the PAM regions.

Table 1. Sequence of guide RNAs.

Sr. No	Name	Sequence
1	gRNA 1	5'AAACAAAGGACGTCCCGCGCAG G3'
2	gRNA 2	5'CGCCGACGGGACGTAAACAAAG G3'

Sequence in red=PAM sequence

The plasmids were received in the form of agar stabs (figure 1). Following the Add gene instructions, those were temporarily stored at 4 ºC. Bacterial inoculum utilized for liquid cultures are shown below in Figure 2.

Plasmid-Design & Construction of anti-HBV CRISPR/CAS9 system

Gene sequence of *HBX* (Gene ID: 944566) and HBV genome sequence (NCBI Reference Sequence: NC_003977.2) were downloaded from NCBI. *HBX* gene sequence was selected for finding suitable CRISPR for which potential 20-base sequences on the HBV were searched by using CRISPR RGEN web tool which is suitable and most used tool used for this purpose. Two suitable targets **(20 nt followed by a PAM sequence)** were selected and it was ensured that these have fewest potential off-target matches throughout the selected host genome [5].

In-silico cloning of gRNA in PX260 (empty Vector)

Both the selected gRNAs were cloned in empty vector PX260. The *in-silico* software "snapgene" was used to clone gRNA (figure 3). The empty vector sequence was opened in the snapgene, Restriction cloning option was selected then gRNA was inserted in the given space and cloned at Bbs1 sites right after the U6 promoter. The cloned sequence was retrieved shown in Figure 4. The sequence was then sent for commercial synthesis to get cloned vector for further experiments.

DNA-custom cloning

Plasmid sequence construct with cloned guide RNA sequence (*in-silico* cloning) was sent for synthesis to "DNA custom cloning" company (USA).

Bacterial Culturing on Agar Plates

The plasmid received was cloned in the bacteria spread on agar plates. Single colony of those bacteria was selected and inoculated in 1.5 mL of LB(liquid) media containing 50 µL ampicillin. The culture was incubated overnight at 37℃ in a shaking incubator (figure 4**).** The LB agar plates having ampicillin selection were prepared. Overnight grown culture was taken and spread on ampicillin positive LB agar plates with the help of a sterilized loop. The streaking was done in the form of 4-quadrant. The streaked plate was incubated overnight culturing at 37ºC.

Plasmid Propagation in E. coli (DH5alpha)

Bacterial Transformation

The concentrated plasmid was then propagated in bacterial cells. Heat-shock transformation method was used to transform the competent cells.

Heat-shock Transformation

The already prepared competent cells (50 µL) were taken from the repository within a 1.5 mL tube. Total 5 µL plasmid was taken to transform those competent cells and was mixed gently in the competent cells followed by incubation on ice for 40 mins. Subsequently the mixture was subjected to heat shock, given at 42 ºC for 90 secs and was again placed on ice for 5 min. Later, 800 µL of LB broth was added to it, mixed well and incubated at 37C for an hour. Finally, 200 µL of transformed cells were spread on LB agar plate (Amp +ve). The ampicillin negative LB agar plates were used as control. The plates were then left for Incubation at 37 ºC overnight. Next day, a few isolated colonies were observed on the agar plate as shown in Figure 5. Some of those were selected randomly and used for further confirmation analysis.

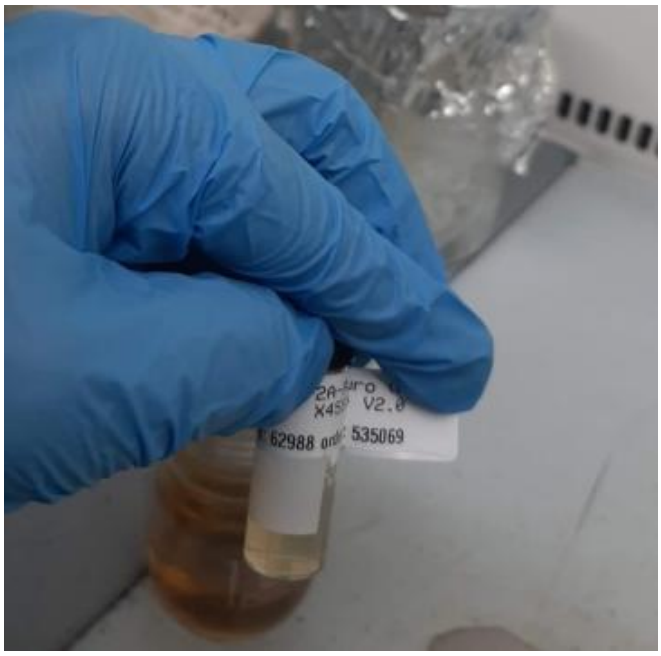

Figure 1. Plasmids received in transformed DH5alpha (Agar Stabs).

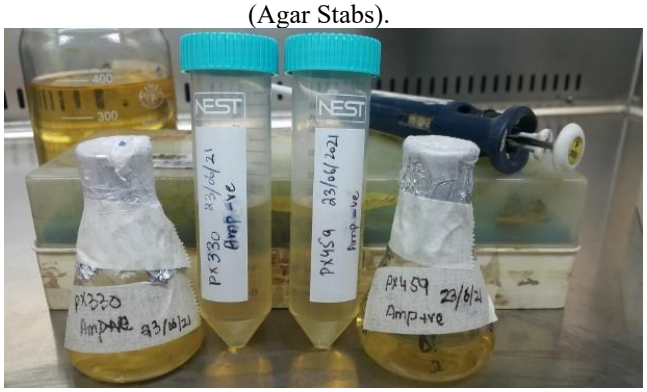

Figure 2. Bacterial Inoculum in LB Broth.

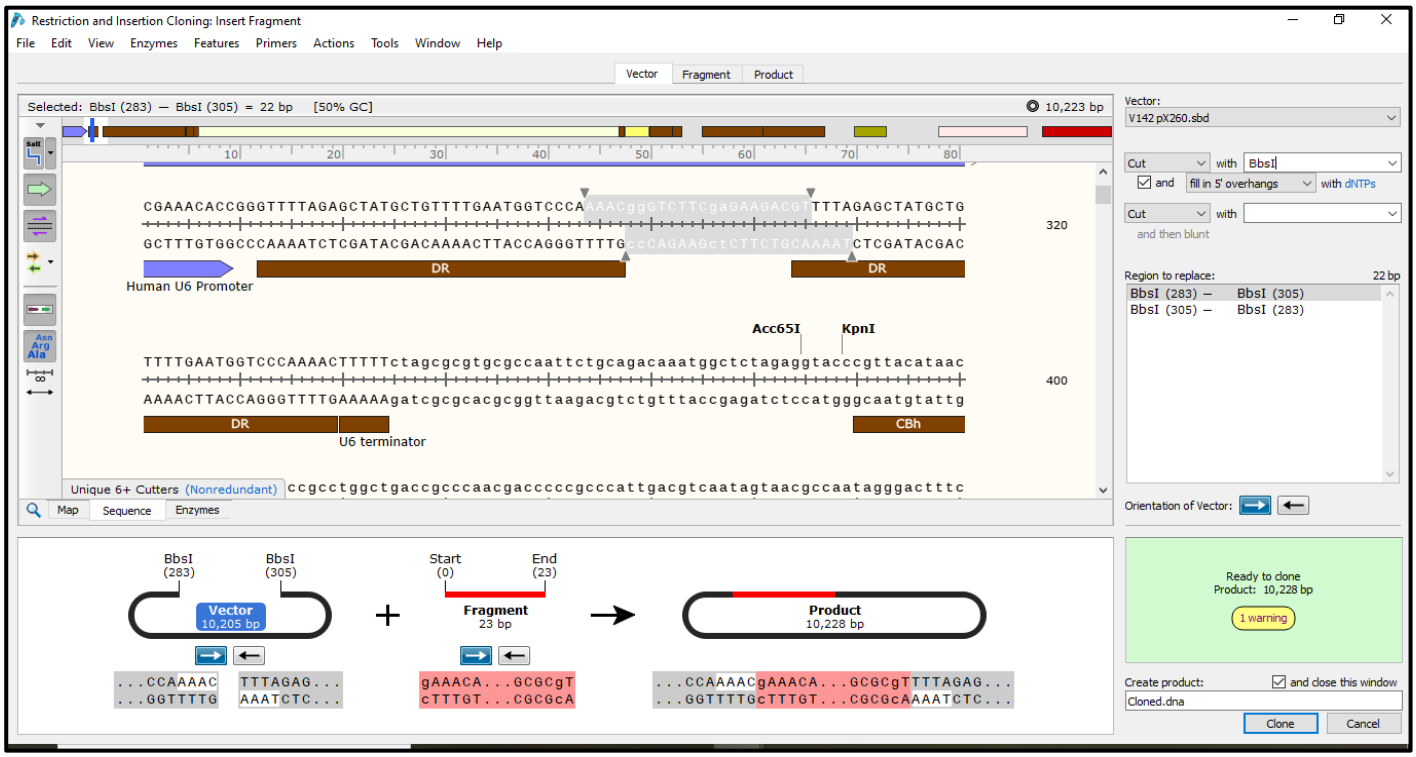

Figure 3. *In-silico* cloning reaction performed by restriction digestion at BbsI site and cloning of 20bp guide RNA.

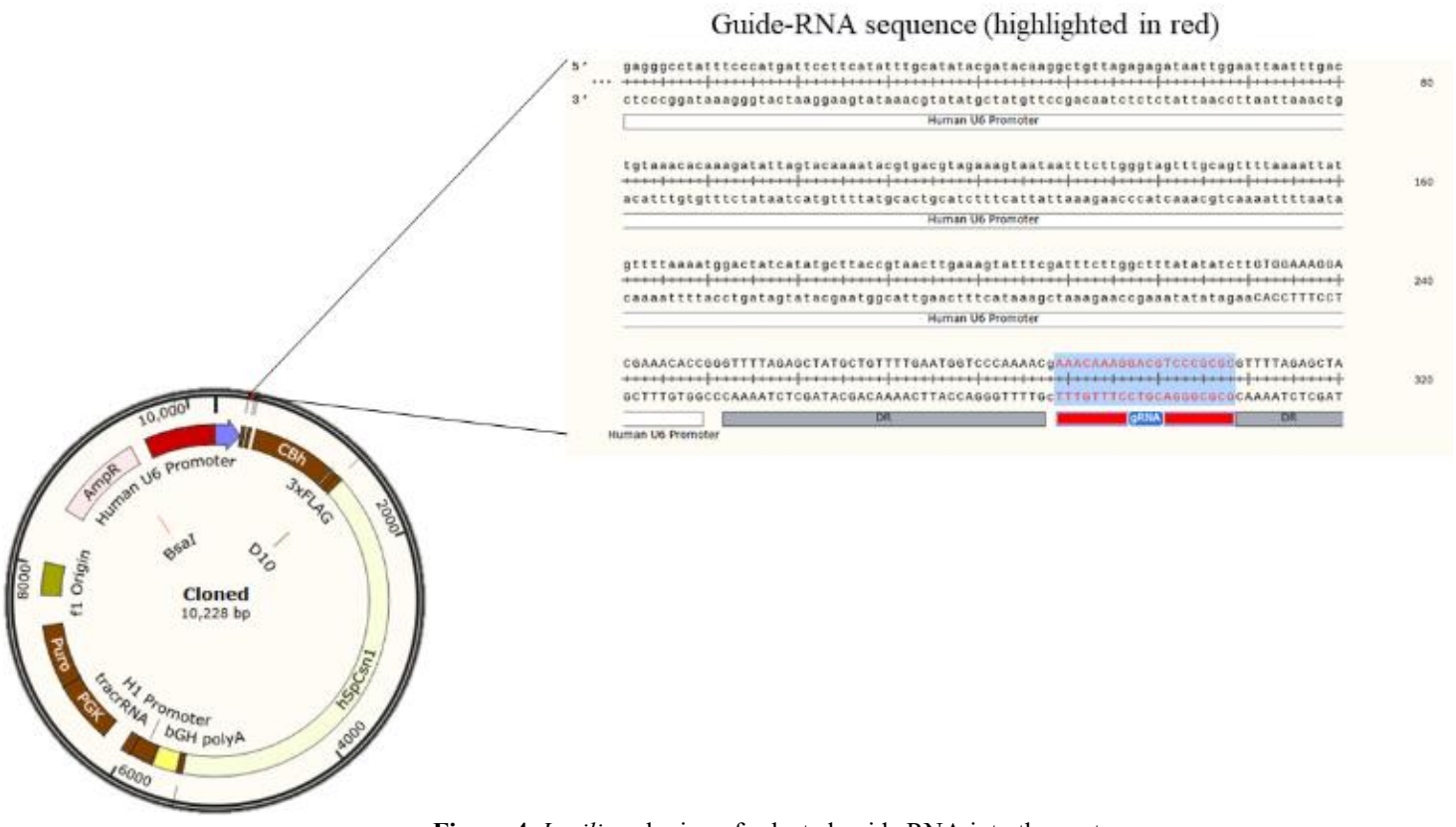

Figure 4. *In silico* cloning of selected guide RNA into the vector.

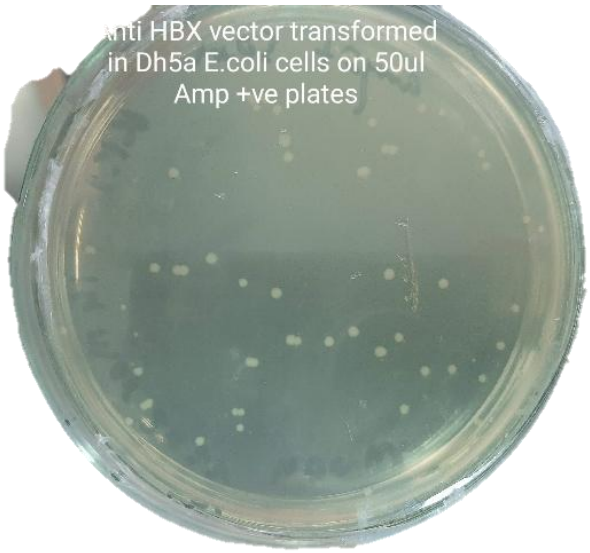

Figure 5. Bacterial colonies recovered on agar plates (ampicillin +ve).

Cell culture testing on Huh-7it cells

Huhit cells cultured in 5 mL media containing DMEM media, 10% FBS (50ml), 1% essential amino acid, antibiotic (streptomycin). After 24 hours the cultures were observed continuously for confluency until 80-90% confluent culture was obtained. For cell splitting, the media was discarded and the cells were washed with PBS (10 mL) twice. Then 1 mL of trypsin was added and mixture was incubated for 4 min at 37 ºC. DMEM (8mL) was added and again subjected to centrifugation at 1200 rpm for 4 min. After cells transfection, supernatant was collected at 24hr and 48hr stage and the media was changed. The supernatant was collected to determine the protein expression by the transformed cells.

Lipofectamine mediated Transfection (Protocol)

Plasmid transfections in Huh7it cells were seeded in the 24 well plate (without antibiotic) at $6x10^4$ cells/ml, left in incubator for 12-24hr. The wells were washed with 1xPBS (500 µL) and about 500 µL fresh serum free media (Opti MEM) was added. The plasmid (1 µL) was diluted in 250 µL Opti MEM media. (At the same time 2 µL of lipofectamine was diluted by addition of 250 µL Opti MEM). The mixture was incubated at room temperature for 5 mins. Mix both the dilutions (plasmid+lipofectamine diluted in OptiMEM) drop by drop. Later, 500 µL DMEM media was added to this mixture for transfection purpose drop wise to the cell. The mixture was shaken well by hand (swirl) before subjecting to overnight incubation. The media was changed the next day (after 24 hr). The cells were observed for any damaging effects or stress induced by transfection under microscope.

Sequence Analysis by Sanger sequencing

After plasmid extraction, sanger sequencing was performed using guide RNA specific primers (forward and reverse) for confirming the plasmid transfection into Huhit7 cells. Applied Bio system (AB sequencing) was used utilized for this purpose.

Results

Plasmid Isolation and Confirmation

The extracted plasmid was then run on agarose gel. The gel was visualized under gel doc (UV Illuminator) (Figure 6).

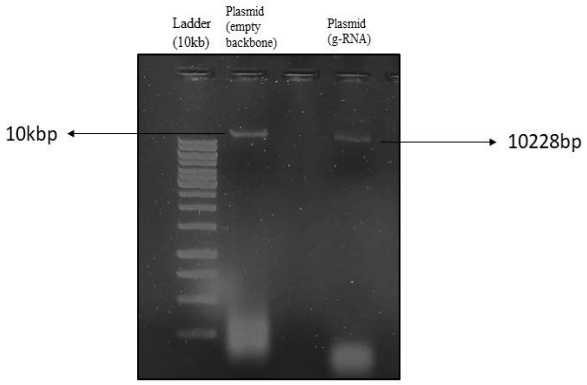

Figure 6. Gel electrophoresis image of Isolated plasmid PX260 (cloned vector), size 10,228bp shown with 10kb ladder.

Plasmid Quantification through Nano drop

The concentration of the plasmid was checked using nano-drop. About 1 µL of TE buffer was used as a control. 1 µL of extracted sample was poured on the optical fibers of the nano-drop machine. The concentrations of the plasmid are as shown in Table 2

Table 2: Nanodrop values for plasmid.

Plasmid	Concentration (ng / µL)	A260/280	A260/230
PX260 (Empty Vector)	36.59	1.80	1.92
PX260 (Cloned Vector)	62.85	1.88	1.65

Potential Off-Target Analysis

The potential off-target analysis performed using (www.rgenome.net/). There was no off target obtained. The guide RNA sequence was used without PAM sequence, for off target prediction The screen-shot of the analysis shown below in Figure 7.

Lipofectamine mediated Transfection

Lipofectamine mediated transfection was carried out in Huhit cells in six well plate seeded. While Figure 8a, b gives the image for cell counting done on a cell counter grid

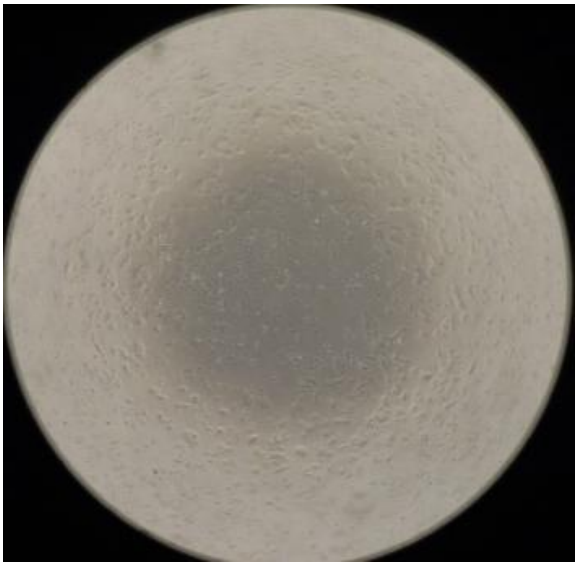

Figure 8(a). Microscopic image of Huh7 it cells

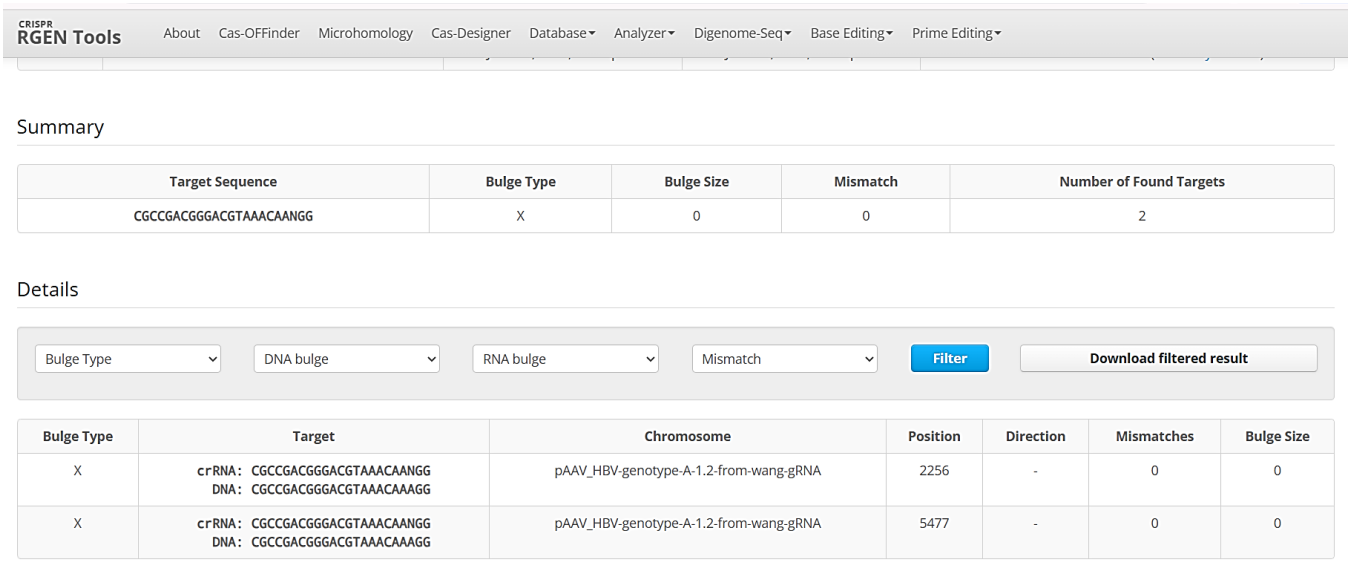

Figure 7. Potential off targets obtained, after RGEN tool for CRISPR-guide RNA analysis.

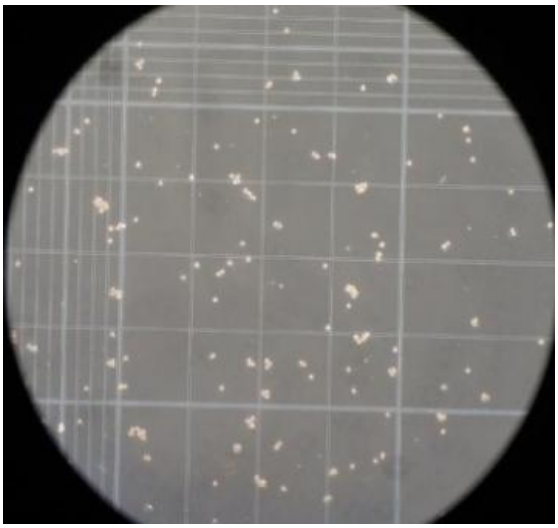

Figure 8(b). Huh7it cells counting (seeded six well) of cells in 6 well plate.

RNA extraction from supernatant

Total RNA extraction was performed using total RNA extraction kit (RNeasy Kit QIAGE, Cat no. 74104). The extracted RNA proceeded for cDNA synthesis using random primers. Figure 10 below gel electrophoresis image. For monitoring the quantity and quality of RNA extracted from cells nanodrop values are given below in table 3. However, figure 9 below indicates the gel electrophoresis image after c-DNA synthesis (table 4) PCR reaction mix are provided as follows.

Table 3. Nanodrop values for the quantity of RNA extracted from transfected cells

Vector	Quantity	A260/280	A260
KKV(cloned vector)	73.9ng/ul	2.56	1.84
KKV(cloned vector)	25ng/ul	2.55	0.68
VO (empty vector)	31.6ng/ul	2.49	0.79
Control (1)	72.2ng/ul	2.70	1.8
Control (2)	42.9ng/ul	2.23	1.07

Table 4. cDNA synthesis PCR reaction mix along with quantities.

Reagents	Quantity
DNA remover	2ul
Random primers	1ul
RT mastermix	2ul
Sample	7ul
Total reaction volume	12ul

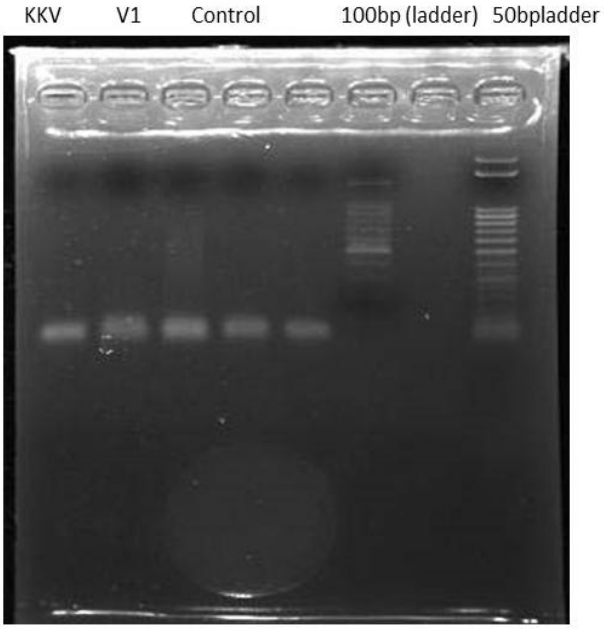

Figure 9. Gel electrophoresis image of cDNA synthesis PCR product (1%agrose gel).

Sequencing Confirmation- (Sanger sequencing)

The sequencing was performed with specific g-RNA primers in order to confirm the successful transfection of plasmids inside mammalian cells. The transfection confirmation is done through plasmid isolation after 48hr of Lipofectamine mediated transfection and further pursued with sequencing analysis shown below (Figure 10)

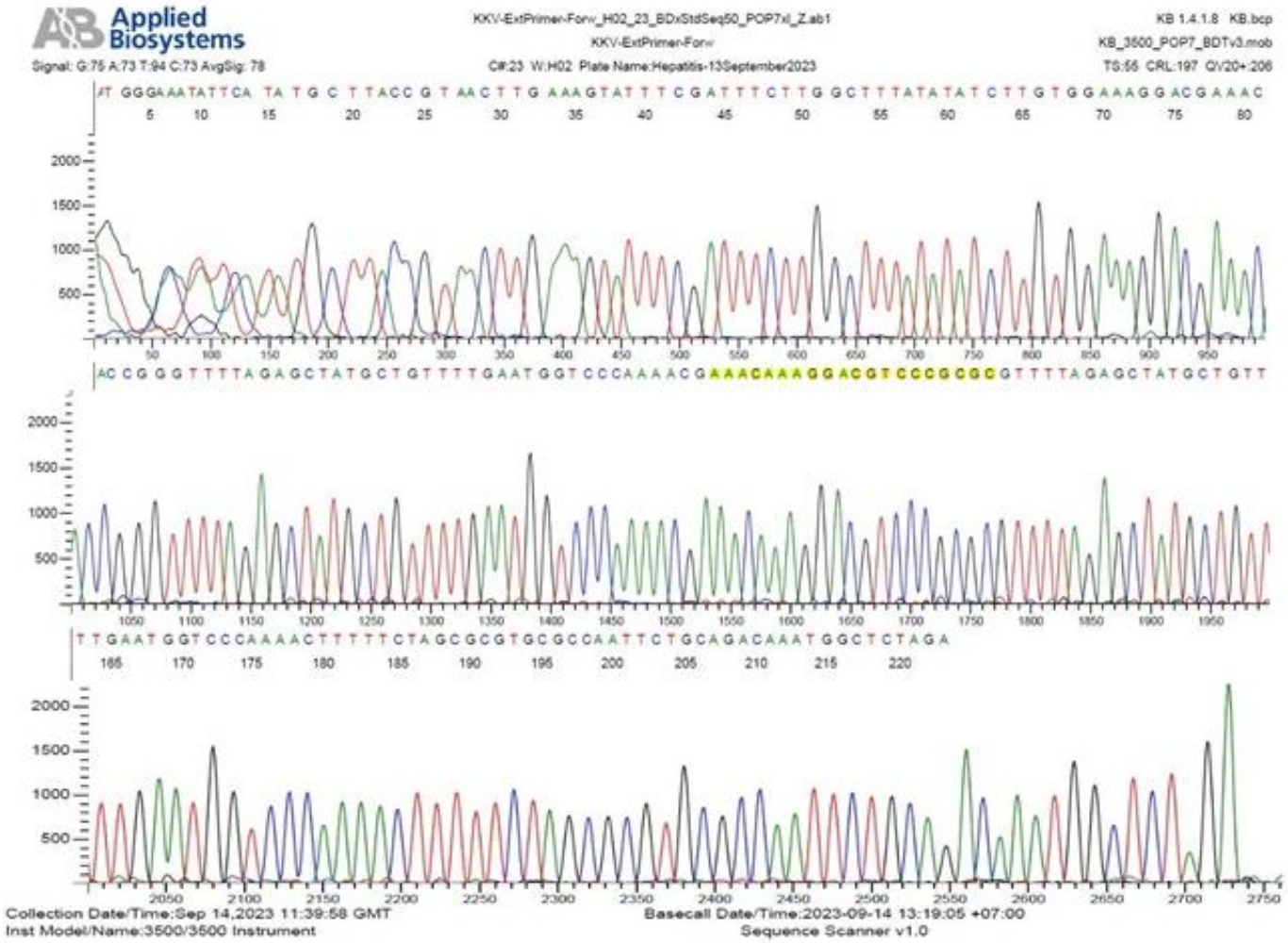

Figure 10. Sanger sequence analysis performed for plasmid guide RNA sequence confirmation. The highlighted sequence is the guide RNA.

Discussion

Over 350 million individuals are chronically infected with HBV, and about 2 billion people have had an HBV infection in the past. Population has been divided according to three endemicity levels; low (greater than 2%), intermediate (from 2% to 7%), and high endemicity (less than equal to 8%).[6] In 2015, approximately, new 1.75 million HCV cases were reported [7]. With 9 million people affected, hepatitis B virus infection is widely reported in Pakistan. Lack of sufficient healthcare facilities and public knowledge are to blame for its rise in Pakistan. In Pakistan, the carrier rate is 3% to 5%. Pakistan has a prevalence of roughly 63.71% of genotype D [8]. Currently, there are two antiviral treatment options for chronic hepatitis B (CHB): nucleos(t)ide analogue (NA) and interferon-alpha (IFN-α) [3]. Despite their effectiveness, neither of them has long-lasting, satisfying off-therapy reactions. However more efficient delivery system like nanoparticles based delivery of therapies are the key area to be explored. Viral vectors have been widely used in recent years to transport CRISPR cassettes both in vitro and in vivo,[9] primarily because of their high gene delivery efficiency and steady transgene expression over the long term[10-12]. The varied tissue tropism of AAV serotypes, in particular, allows AAV to be flexibly built to target particular organs or tissues [13, 14]. Ramanan et al, in 2015 demonstrated that two of the sgRNA/Cas9 combinations showed decreased production of pgRNA and HBV viral antigens. They infected the cultured NTCP-expressing HepG2 cells with patient-derived HBV. The effect of two pairs of sgRNA and cas9 was observed and the results showed reduced productive infection and HBV replication. After hydrodynamic injection of mice with the pairs, robust reduction in circulating viral particles by up to 95% of the controls were observed. Production of viral mRNA and secretion of HBeAg was also observed to be reduced by more than 50% [15].

Acknowledgments

We would like acknowledge Hepatitis Laboratory of Universities Airrlanga (Indonesia) for their support during cell culture experiments.

References

1. Lv, W., et al., The Application of the CRISPR/Cas9 System in the Treatment of Hepatitis B Liver Cancer. Technology in Cancer Research & Treatment, 2021. 20: p. 15330338211045206.
2. Schweitzer, A., et al., Estimations of worldwide prevalence of chronic hepatitis B virus infection: a systematic review of data published between 1965 and 2013. The Lancet, 2015. 386(10003): p. 1546-1555.

3. Yang, H.-C. and J.-H. Kao, Revisiting the natural history of chronic HBV infection. Current Hepatology Reports, 2016. 15(3): p. 141-149.
4. Yang, H.-C. and P.-J. Chen, The potential and challenges of CRISPR-Cas in eradication of hepatitis B virus covalently closed circular DNA. Virus research, 2018. 244: p. 304-310.
5. Hsu, P.D., E.S. Lander, and F. Zhang, Development and applications of CRISPR-Cas9 for genome engineering. Cell, 2014. 157(6): p. 1262-1278.
6. Te, H.S. and D.M. Jensen, Epidemiology of hepatitis B and C viruses: a global overview. Clinics in liver disease, 2010. 14(1): p. 1-21.
7. Blach, S., et al., Global prevalence and genotype distribution of hepatitis C virus infection in 2015: a modelling study. The lancet Gastroenterology & hepatology, 2017. 2(3): p. 161-176.
8. Idrees, M., S. Khan, and S. Riazuddin, Common genotypes of hepatitis B virus. Journal of the College of Physicians and Surgeons--pakistan: JCPSP, 2004. 14(6): p. 344-347.
9. Li, L., S. Hu, and X. Chen, Non-viral delivery systems for CRISPR/Cas9-based genome editing: Challenges and opportunities. Biomaterials, 2018. 171: p. 207-218.
10. Heckl, D., et al., Generation of mouse models of myeloid malignancy with combinatorial genetic lesions using CRISPR-Cas9 genome editing. Nature biotechnology, 2014. 32(9): p. 941-946.
11. Yu, W., et al., Nrl knockdown by AAV-delivered CRISPR/Cas9 prevents retinal degeneration in mice. Nature communications, 2017. 8(1): p. 14716.
12. Shalem, O., et al., Genome-scale CRISPR-Cas9 knockout screening in human cells. Science, 2014. 343(6166): p. 84-87.
13. Zincarelli, C., et al., Analysis of AAV serotypes 1–9 mediated gene expression and tropism in mice after systemic injection. Molecular therapy, 2008. 16(6): p. 1073-1080.
14. JM, G.G.V.L.W., New recombinant serotypes of AAV vectorsCurr. Gene Ther, 2005: p. 5285-297.
15. Ramanan, V., et al., CRISPR/Cas9 cleavage of viral DNA efficiently suppresses hepatitis B virus. Scientific reports, 2015. 5(1): p. 1-9.

Novel Titanium Carbide (Ti3C2Tx) MXene electrocatalyst for HER application.

Muhammad Yameen Solangi[1*], Abdul Hanan[2], Umair Aftab[1], Imtiaz Ali Soomro[1], Zafar Hussain Ibupoto[3],

[1]Department of Metallurgy and Materials Engineering, Mehran University of Engineering and Technology, 76080 Jamshoro, Sindh, Pakistan
[2]Sunway Centre for electrochemical energy and sustainable technology (SCEEST), School of Engineering and Technology, Sunway University, Selangor, Malaysia
[3]Dr. M.A Kazi Institute of Chemistry University of Sindh Jamshoro, 76080, Sindh, Pakistan
Corresponding Authorl: yameen.engineer14@gmail.com
Received: 21-11-2024, Received in Revised form: 08-03-2025, Accepted: 11-05-2025, Published: 30-06-2025

Abstract

Water electrolysis is a promising method for producing green hydrogen (H_2), and two-dimensional (2D) materials are gaining more attention globally, especially in the field of energy conversion/storage devices, because of their special attributes. The goal of this research is to create an electrocatalyst that is cost-effective, long-lasting, and sustainable using two-dimensional (2D) MXene materials from MAX phase. This study emphasized the synthesis of Ti3C2Tx based MXene via etching method. The surface morphology, elemental analysis, surface functionalization, crystalline phase purity, and water splitting behavior of the as-prepared catalyst (Ti_3C_2Tx) has been examined by numerous characterization techniques, including scanning electron microscopy (SEM), Energy dispersive spectroscopy (EDS), Fourier transform infrared spectroscopy (FTIR), X-ray diffraction (XRD), and electrochemical measurement. The robust 2D material (Ti_3C_2Tx) is found to have more effective hydrogen evolution reaction (HER) activity in 1.0 M KOH alkaline media. The electrocatalyst exhibits rapid reaction kinetics having an overpotential of 542 mV at a current density of 10 mA/cm2 accompanied with 170 mV/dec Tafel slope value. Additionally, as demonstrated by effective HER activity, it provides low charge transfer resistance (Rct) together with good stability, high electrochemical active surface area (ECSA), and durability for several hours. Moreover, Ti3C2Tx has superior turnover frequency and theoretical hydrogen production. Henceforth, for industrial-scale energy conversion systems, this innovative electrocatalyst may help to replace those electrocatalyst based on precious metals.

Keywords: Water splitting, Electrocatalyst, Hydrogen evolution reaction, 2D MXene, Alkaline Media

Introduction

The global demand for energy is rising alongside the growing population, leading to an anticipated increase in annual per capita consumption as human lifestyles advance [1-3]. Currently, 80% of the world's energy is derived from fossil fuels, which significantly harm the atmosphere by emitting greenhouse gases, thereby affecting the climate, raising Earth's temperature, and depleting freshwater resources [4]. There is a pressing need to develop more efficient and cost-effective renewable energy sources [5]. Hydrogen (H_2) technologies are gaining traction as a renewable energy option, with H_2 being produced through methods such as steam reforming, thermal decomposition, biomass fermentation, and electrolysis [6-8]. Among these, water electrolysis is particularly appealing because it generates H_2 by splitting water molecules into hydrogen and oxygen (O_2). During this process, two reactions occur: the hydrogen evolution reaction (HER) and the oxygen evolution reaction (OER) [9, 10]. The HER and OER take place at the cathode and anode in acidic and alkaline electrolytes, respectively. However, HER faces more challenges in alkaline environments, necessitating a higher electrical potential to proceed [11]. To address this, noble metal-based electrocatalysts like Platinum (Pt), Ruthenium (Ru), and Iridium (Ir) and their alloys are employed to facilitate the reaction at low overpotential [12]. Despite their effectiveness, these noble catalysts are expensive due to limited availability, making them less viable for large-scale production. Consequently, there is a global focus on developing new methods that are reliable for industrial-scale H_2 production [13]. In this context, two-dimensional (2D) materials have been developed and are widely used for energy storage and conversion applications [14]. Among these, MXene is a novel material known for its high electrical conductivity and adjustable surface functionality [15]. MXene is derived from the MAX phase, with the general formula $M_{n+1}AX_n$ (n = 1, 2, 3), where M represents transition metals, A denotes IIIA or IVA elements, and X indicates nitrogen or carbon [16, 17]. To produce MXene, the A layer (such as Al, Ga) is selectively removed and replaced with Tx functional groups (-O, -OH, and -F). $Ti_3C_2T_x$ MXene is predominantly used in H_2 generation applications due to its excellent metallic conductivity and hydrophilicity [18, 19]. Recent literature reports various thin-layered $Ti_3C_2T_x$ MXene electrocatalysts for HER activity, such as MoS_2/Ti_3C_2 [20], Fe/Ni doped GO@ $Ti_3C_2T_x$ [21], and1T/2H MoS_2 (25D)/ $Ti_3C_2T_x$-1 [22]. However, MXene nanosheets exhibit strong intermolecular attraction, leading to restacking or reaggregation after dehydration, which significantly reduces the number of electrocatalytically active sites [23]. Therefore, it is crucial to develop combinations with MXene that preserve its thin-layered, delaminated structure.

This research presents a promising method for synthesizing $Ti_3C_2T_x$ using an acid etching technique, where $Ti_3C_2T_x$ is derived from Ti_3AlC_2 through the use of HCl and HF acids. Various physicochemical methods were employed to investigate the structural, compositional, and morphological properties. The newly synthesized catalyst, along with the MAX phase material, was evaluated for its HER activity in a 1.0 M KOH solution. The MXene demonstrated superior electrochemical performance, with an overpotential of 542 mV at a current density of 10 mA/cm^2, a Tafel slope of 170 mV/dec, and stability for 15 hours. This approach is entirely novel and has not been previously documented.

Experimental Works

MAX phase (Ti3AlC2), Hydrofluoric acid (HF), Potassium hydroxide (KOH), Hydrochloric acid (HCl), 5 wt% Nafion, and Deionized (DI) water were sourced from Sigma Aldrich in Karachi, Pakistan. The experiments utilized high-grade analytical materials without any purification.

The MXene was synthesized using an etching method involving HF and HCl. In this process, the Al layer was removed from the Ti_3AlC_2 MAX phase. Specifically, 0.5g of bulk MAX was gradually added to a Teflon-lined beaker

This work was presented at 4th ASEAN Pakistan Conference on Materials Science (APCOMS), 2025.

containing 60 mL of a solution made up of 20% aqueous hydrofluoric acid and 5% hydrochloric acid. The resulting Ti_3AlC_2 powder was continuously stirred at room temperature for 40 hours using a Teflon-coated magnetic stir bar. This led to the etching and removal of Al layers from the MAX phase. To neutralize the acidic nature of the solution, the HF acidic solutions were repeatedly centrifuged with deionized water until the pH reached approximately 7. The MXene was then collected and dried at room temperature. Consequently, the as-synthesized $Ti_3C_2T_x$ was prepared for characterization and optimization for electrochemical analysis.

To assess the phase purity and crystal orientation of the synthesized nanostructures, Philips PAN analytical X-ray diffraction techniques were employed. The equipment was set to operate at a voltage of 45 kV, a current of 45 mA, and utilized CuKa radiation with a wavelength of 1.5418 °A. The resulting X-ray spectra were analyzed using High Score Plus software. For morphological and elemental analysis of the synthesized materials, JEOL JSM-6480A Scanning Electron Microscopy (SEM)/ Energy Dispersive Spectroscopy (EDS) was conducted at an operating voltage of 20 kV. Additionally, the surface functionalization of the samples was examined through Fourier Transform Infrared (FTIR) Spectroscopy, via PerkinElmer's Spectrum two instrument. Each sample, with a concentration of 0.5 wt%, was mixed with dried KBr for measurement, and the operating range was maintained between 400 and 4000 cm^{-1}.

The electrochemical evaluation for the hydrogen evolution reaction (HER) was conducted using a VERSASTAT4-500 system equipped with a three-electrode cell setup. This setup included a reference electrode (silver/silver chloride), a counter electrode (platinum wire), a working electrode (glassy carbon electrode), and an electrolyte solution of 1.0 M KOH. The GCE was modified with catalyst ink, which was prepared by mixing 5 mg of the synthesized catalyst, 20 µL of a 5% Nafion solution, and 4 mL of deionized water. The mixture was thoroughly dispersed using an ultrasonic bath for 25 minutes. The resulting uniform ink was applied to the cleaned GCE surface and dried by blowing air. The dried GCE was then incorporated into the cell setup for electrochemical testing. The HER polarization curve was initiated using linear sweep voltammetry in 1.0 M KOH at a scan rate of 5 mV/s. To assess the durability of the optimal sample, a chrono-potentiometric test was conducted at current densities of 10 mA/cm² and 20 mA/cm² for 30 hours. Electrochemical impedance spectroscopy (EIS) was employed to analyze the charge transfer resistance (Rct) of the various synthesized catalysts, operating at -0.4 V vs RHE with a 5 mV sinusoidal potential across a frequency range from 100,000 Hz to 1 Hz. The electrochemical active surface area (ECSA) of the samples was determined using cyclic voltammetry (CV) at different scan rates in the non-faradaic region [24].

Results and discussion

Figure 2 illustrates the unique peak pattern of MAX powder (Ti3AlC2). The XRD patterns of the original MAX powder align well with the reference JCPDS no. 520-875, featuring both sharp and broad peaks at approximately 9.28°, 19.15°, 33.71°, 34.04°, 38.81°, 39.04°, 41.81°, 44.92°, 48.54°, 56.57°, and 60.25°, which correspond to the (002), (004), (100), (101), (008), (104), (105), (106), (107), (109), and (110) crystallographic planes [25, 26]. The XRD diffraction pattern of MXene reveals a prominent peak at 7.22° associated with the (002) plane, along with smaller peaks at 14.4° and 29° corresponding to the (004) and (006) planes, respectively, which are consistent with existing literature [27]. Following the HF+HCl exfoliation treatment, a significant shift in the (002) peak from 2θ 9.26° to 7.22° was observed, indicating an increase in the lattice parameter. The double contribution in single peak is also investigated and a zoomed-in XRD peaks analysis added as sub-figure2(b).

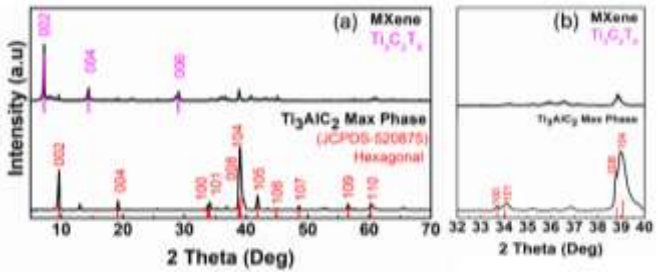

Figure 2. (a) XRD diffraction patterns of MAX Phase and MXene (b) Zoomed-in XRD peaks analysis

SEM analysis was employed to examine the morphology and structural characteristics of Ti_3AlC_2 and exfoliated MXene. Figure 3a [28] illustrates the irregular surface and densely packed structure of the MAX phase. Following HF+HCl treatment of the MAX phase, the MXene exhibited a morphology resembling exfoliated flakes, as shown in Figure 3b [29]. Our successful synthesis of MXene was confirmed through SEM analysis, aligning with the literature provided. The EDS analysis was also performed for elemental analysis. The EDS spectra of MAX phase contain C, Al and Ti elements with 8.77, 16.52 and 74.71% mass percentage as given Figure 3a. While the EDS spectra of MXene comprises C, F, Al and Ti elements with 5.16, 9.96, 0.66 and 84.22% mass percentage mentioned in Figure 3b. It can be observed that the mass percentage of Al is reduced from 16.52 to 0.66 % in MXene which validates the leaching of Al from MAX phase.

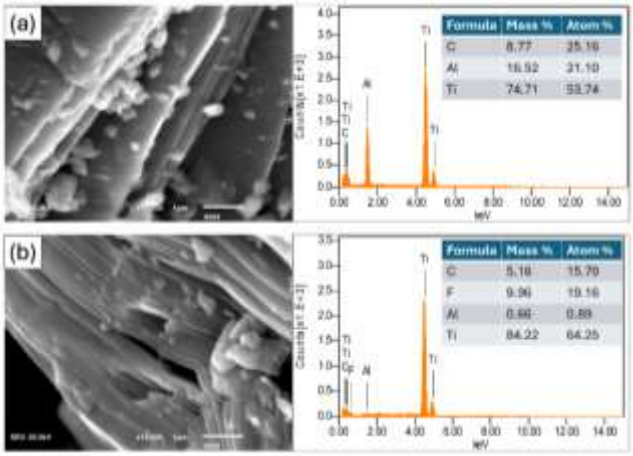

Figure 3. SEM micrographs and corresponding EDS spectra: (a) Ti3AlC2 (MAX) and (b) Ti3C2Tx (MXene)

FTIR spectroscopy was employed to examine the surface functionalization of the synthesized materials. Figure 4 displays the FTIR spectra for Ti_3AlC_2 (MAX) and $Ti_3C_2T_x$ (MXene). It was noted that all the materials exhibited

several common bands, specifically at 1382, 1601, 2854, 2930, and 3438, cm^{-1}, which correspond to (C-H), (O-H), (C-H), (C-H), and (O-H), respectively. The O-H groups are present due to the absorption of external water (H_2O) molecules on the material surfaces, attributed to their hydrophilic nature. The C-H bands in the materials are linked to the symmetrical/asymmetrical stretching of methylene (CH_2) and methyl (CH_3) groups [29, 30]. Additionally, the FTIR spectra of the Ti_3AlC_2 phase likely indicate Ti- Ti-O and O-Ti deformation vibration bonding at 605 and 879 cm^{-1}, respectively. Furthermore, the peaks at 481 cm^{-1} are indicative of the twisting vibration of Ti-C. In contrast, the $Ti_3C_2T_x$ exhibited a fluorine-terminated band (C-F) at 1108 cm^{-1} and a pronounced Ti-C band, confirming the etching of the Ti_3AlC_2 MAX phase.

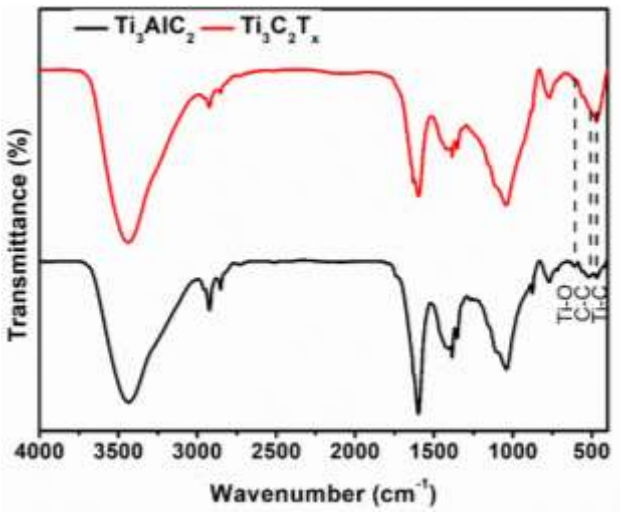

Figure 4. FTIR spectrum of Ti3AlC2 , and Ti3C2Tx

The electrochemical evaluation of Ti_3AlC_2 and $Ti_3C_2T_x$ is depicted in Figure 5. These electrocatalysts were subjected to HER analysis using LSV in a 1.0 KOH media, as illustrated in Figure 5(a). The LSV curve indicates that the $Ti_3C_2T_x$ exhibits an overpotential of 542 mV, while Ti_3AlC_2 shows a higher overpotential of 676 mV at 10 mA/cm^2 current density. The overpotential values for each catalyst are displayed in a histogram in Figure 5(b). The correlation between reaction rate and applied overpotential provides insights into the electrocatalysts' electrochemical performance, as indicated by the Tafel slope in Figure 5(c). The Tafel slopes for Ti_3AlC_2 and $Ti_3C_2T_x$ are 214 and 170 mV/dec, respectively. In an alkaline setting, the HER reaction kinetics are described by three sequential steps reported in literature [31-33].

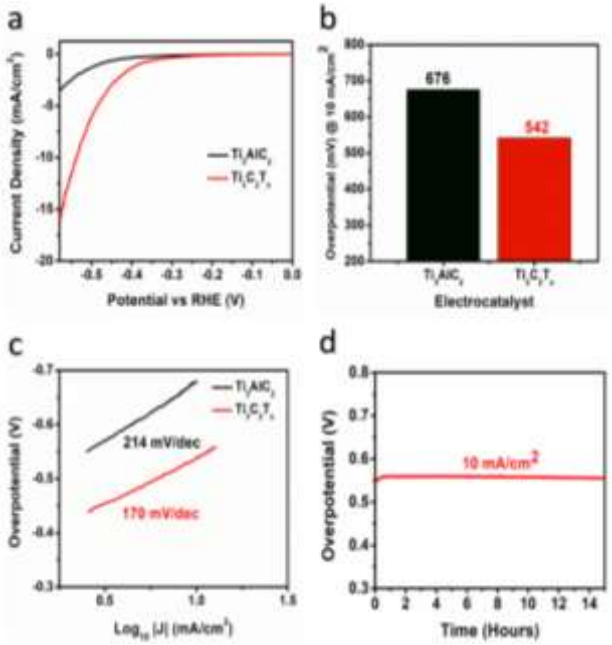

Figure 5. (a) LSV of different catalyst (b) Histogram of overpotentials of catalysts (c) Tafel slope values (d) Chronopotentiometric durability.

The durability of the MXene electrocatalyst has been assessed through the chronopotentiometry test, as depicted in Figure 5(d). The durability of an electrocatalyst is crucial for practical applications [34]. Therefore, the MXene material's stability was evaluated using chronopotentiometry at a current density of 10 over a period of 15 hours, confirming its extended-period electrochemical performance. It is important to note that the anticipated electrocatalyst has shown stability, as illustrated in Figure 5(e).

EIS has been carried to evaluate the charge transfer resistance (Rct) of different electrocatalysts in a 1 M KOH electrolyte. Figure 6 (a) illustrates the Nyquist and Bode (I and II) plots. When compared to MAX (Ti_3AlC_2), MXene ($Ti_3C_2T_x$) shows an enhanced phase angle in Figure 6 (a). Furthermore, the Rct values for Ti_3AlC_2 and $Ti_3C_2T_x$ have been determined to be 2825 and 1705 Ω, respectively. As indicated in Table.1, MXene's lower Rct suggests superior electrical conductivity, which enhances its electrochemical performance relative to its counterparts.

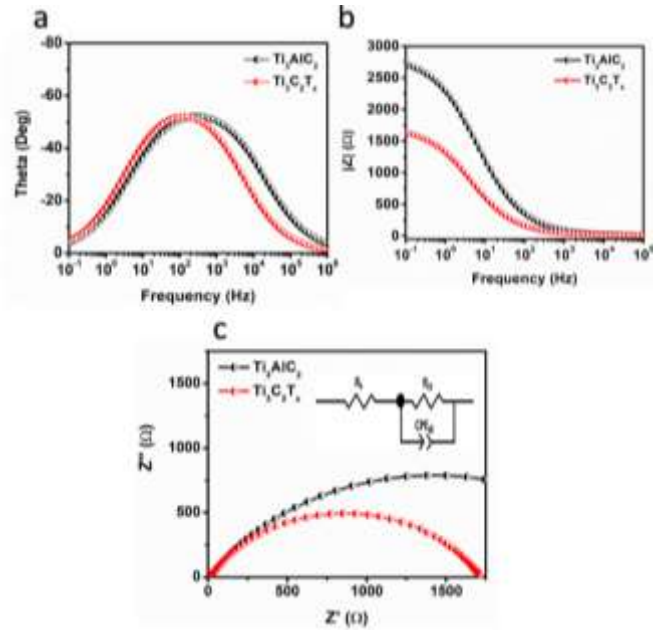

Figure 6. EIS data of Ti_3AlC_2, and $Ti_3C_2T_x$ showing (a &b) Bode plot and (c) Nyquist plot.

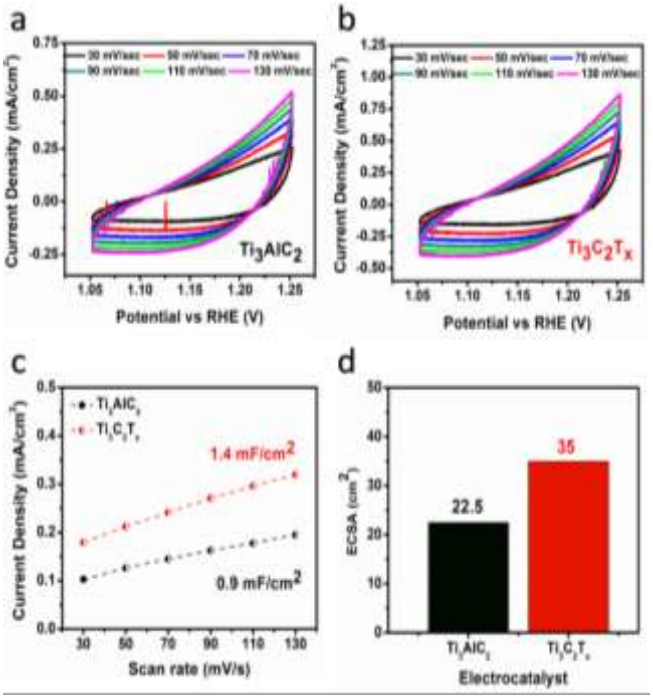

Figure 7. CV data (a, & b) of catalyst (c) C_{dl} data of prepared catalyst (d) ECSA calculated from C_{dl}.

Additionally, cyclic voltammetry (CV) has been applied to examine the double-layer capacitance (Cdl) in the non-faradic region of the synthesized electrocatalyst, as illustrated in Figure 7 (a & b). This analysis utilized various scan rates, specifically 30, 50, 70, 90, 110, and 130 mV/s. The calculated Cdl values are 0.9 and 1.4 μF/cm^2 for Ti_3AlC_2 and $Ti_3C_2T_x$, respectively, as represented in Figure 7 (c). Furthermore, the electrochemical active surface area (ECSA) was determined using the Cdl values through the formula provided.

$$ECSA=Cdl/Cs \quad (4)$$

In equation (4), Cdl denotes the double-layer capacitance, whereas Cs refers to the specific capacitance at the electrolyte interface. It is important to note that the Cs value is 0.04 mF/cm^2 for 1 M KOH media. The ECSA values for $Ti_3C_2T_x$ and Ti_3AlC_2 have been calculated as 35 and 22.5 cm^2, respectively, as shown in Figure 7(d). The comparative analysis with literature is given in Table. 2.

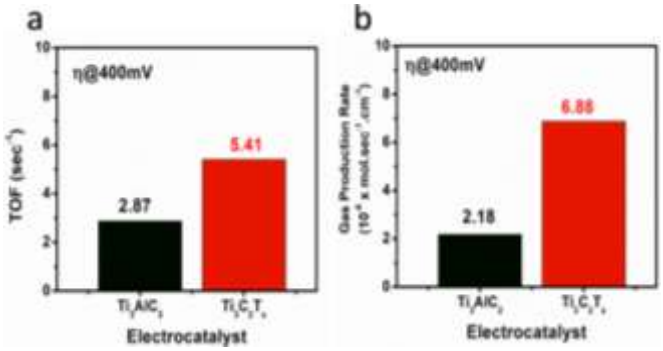

Figure 8. (a) Turnover Frequency at 400 mV overpotential (c) H_2 production @ fixed 400 mV overpotential

The turnover frequency (TOF) for different electrocatalysts is determined at a constant overpotential of 400 mV, as illustrated in Figure 8 (a). The current densities and corresponding TOFs for $Ti_3C_2T_x$ and Ti_3AlC_2 are 1.32 mA/cm^2 and 5.41 s^{-1}, and 0.42 mA/cm^2 and 2.87 s^{-1}, respectively. This suggests that CT-30 has the potential to significantly excel in industrial applications. To support this, theoretical H_2 production is also calculated to confirm the electrocatalyst's gas production rate.

Figure 8 (b) illustrates the hydrogen gas production rates for different catalysts. The findings indicate that MXene achieves a superior hydrogen production rate of 6.88x10^{-6} mol/s.cm compared to the others. This enhancement likely boosts the performance of this composition, making it a promising candidate for HER activity in KOH media. Table.1 presents various electrochemical characteristics of the prepared materials. In summary, MXene demonstrated strong electrochemical performance, aligning with recent research findings.

Table I
Concise features of prepared catalysts for HER application.

Catalyst	LSV data		EIS data		CV data	
	Overpotential	Tafel Slope	Charge Transfer Resistance	Double Layer Capacitance	Double Layer Capacitance	Electrochemically active surface area
	η_{10} (mV)	B (mV/dec)	R_{ct} (Ω)	CPE_{dl} (mF)	C_{dl} (μF/cm^2)	ECSA (cm^2)
Ti_3AlC_2	676	214	2825	0.01	0.9	22.5
$Ti_3C_2T_x$	542	170	1705	0.03	1.4	35

Table II
Comparative Analysis with Literature

Catalyst	R_{ct} *(Ω)*	ECSA *(cm^2)*	References
$Ti_3C_2T_x$	30.04	2.31	[35]
$Ti_3C_2T_x$	512	72.5	[36]
$Ti_3C_2T_x$	1705	35	This Work

5. Conclusion

To conclude, the electrocatalysts discussed were successfully created using an aqueous chemical growth technique. The two-dimensional material $Ti_3C_2T_x$ was synthesized with success. The physical and electrochemical properties of the synthesized material, along with its MAX phase, were examined using numerous analytical methods. MXene demonstrated a lower overpotential of 542 mV at 10 mA/cm^2 current density compared to the MAX sample in an alkaline electrolyte. Furthermore, the low Tafel slope of MXene, approximately 170 mV/dec, further enhanced its HER activity. It was observed that the MXene catalyst remained durable and stable at a current density of 10 mA/cm^2 for 15 hours without any potential drop. The 2D structure of $Ti_3C_2T_x$ facilitated easy charge carriage, resulting in a low charge transfer resistance (Rct) of 1705 Ω, a higher double layer capacitance (Cdl) of 1.4 μF/cm^2, and a greater electrochemical active surface area (ECSA) of 35 cm^2. Consequently, this enhances the sturdiness of the hydrogen evolution reaction (HER), which is advantageous for energy production applications.

Author Contributions

Muhammad Yameen Solangi, prepared desired material, analyzed initial HER test, and written part of the manuscript, Abdul Hanan investigated physical tests FTIR and written his part, Imtiaz Ali Soomro written the manuscript part with some post characterizations such as Chronopotentiometry and other physical tests, Zafar Hussain investigated physical tests (SEM/EDS) and partially supervised the work, Umair Aftab overall supervised the work and written relevant part of the manuscript.

Acknowledgement

The authors would like to express their heartfelt gratitude to the department of Metallurgy & Materials Engineering, Mehran University of Engineering & Technology, Jamshoro.

Conflicts of Interest

The authors of this paper have acknowledged no conflicts of interest.

References

1. R. Badrnezhad, et al., "Effect of iron on Ni–Mo–Fe composite as a low-cost bifunctional electrocatalyst for overall water splitting", International Journal of Hydrogen Energy, Vol. 46, no. 5, pp. 3821-3832, 2021.
2. Y. A. Bhutto, et al., "Investigating the optical absorption and thermal conductivity of nano-enhanced lauric acid phase change material for energy storage application", in IOP Conference Series: Earth and Environmental Science, 2023. IOP Publishing.
3. Y. A. Bhutto, et al., "Thermal behaviour of Paraffin-MWCNT stabilized by Sodium dodecylbenzene sulphonate nano-enhanced phase change material for energy storage applications", in IOP Conference Series: Earth and Environmental Science, 2023. IOP Publishing.
4. A. Islam, et al., "Shape stable composite phase change material with improved thermal conductivity for electrical-to-thermal energy conversion and storage", Materials Today Sustainability, Vol. 25, p. 100678, 2024.
5. Y. A. Ali Bhutto, et al., "Electrical and thermal performance assessment of photovoltaic thermal system integrated with organic phase change material", 2024, Vol. 488, p. 01007.
6. U. Aftab, et al., "Mixed CoS2@Co3O4 composite material: An efficient nonprecious electrocatalyst for hydrogen evolution reaction", International Journal of Hydrogen Energy, Vol. 45, no. 27, pp. 13805-13813, 2020.
7. A. Hanan, et al., "Co2FeO4@ rGO composite: Towards trifunctional water splitting in alkaline media", 2022, Vol. 47, no. 80, pp. 33919-33937.
8. A. Pareek, et al., "Insights into renewable hydrogen energy: Recent advances and prospects", Materials Science for Energy Technologies, Vol. 3, pp. 319-327, 2020.
9. A. J. Laghari, et al., "MgO as promoter for electrocatalytic activities of Co3O4–MgO composite via abundant oxygen vacancies and Co2+ ions towards oxygen evolution reaction", International Journal of Hydrogen Energy, Vol. 48, no. 34, pp. 12672-12682, 2023.
10. P. Banoth, C. Kandula, and P. Kollu, "Introduction to Electrocatalysts", in Noble Metal-Free Electrocatalysts: New Trends in Electrocatalysts for Energy Applications. Volume 2. American Chemical Society, pp. 1-37, 2022.
11. Z. H. Ibupoto, et al., "NiCo2O4 nanostructures loaded onto pencil graphite rod: An advanced composite material for oxygen evolution reaction", 2022, Vol. 47, no. 10, pp. 6650-6665.
12. W. Li, et al., "Defective RuO2/TiO2 nano-heterostructure advances hydrogen production by electrochemical water splitting", Chemical Engineering Journal, Vol. 431, p. 134072, 2022.
13. N. T. T. Thao, et al., "Current Trends of Iridium-Based Catalysts for Oxygen Evolution Reaction in

Acidic Water Electrolysis", 2024, Vol. 4, no. 1, p. 2300109.
14. L. Zhang, et al., "Manganese–cobalt hydroxide nanosheets anchored on a hollow sulfur-doped bimetallic MOF for high-performance supercapacitors and the hydrogen evolution reaction in alkaline media", Dalton Transactions, Vol. 53, no. 3, pp. 1274-1283, 2024.
15. A. Hanan, et al., "Novel rGO@Fe3O4 nanostructures: An active electrocatalyst for hydrogen evolution reaction in alkaline media", Journal of the Indian Chemical Society, Vol. 99, no. 5, p. 100442, 2022.
16. M. Rahman and M. S. Al Mamun, "Future prospects of MXenes: synthesis, functionalization, properties, and application in field effect transistors", Nanoscale Advances, Vol. 6, no. 2, pp. 367-385, 2024.
17. S. B. Devi and R. Navamathavan, "One-Pot Hydrothermal Synthesis of Ti3C2 (MXene)-CoS2 Nanocomposite as a Bifunctional Electrocatalyst (HER/OER) for a Clean Environment", Journal of the Electrochemical Society, Vol. 170, no. 9, 2023.
18. D. Liu, et al., "Nitrogen-Doped MoS2/Ti3C2TX Heterostructures as Ultra-Efficient Alkaline HER Electrocatalysts", Inorganic Chemistry, Vol. 60, no. 13, pp. 9932-9940, 2021.
19. L. P. Hao, et al., "Synergistic Integration of MXene and Metal-Organic Frameworks for Enhanced Electrocatalytic Hydrogen Evolution in an Alkaline Environment", 2023, Vol. 13, no. 5, p. 802.
20. S. K. Raj, et al., "Three-dimensional Ni/Fe doped graphene oxide @ MXene architecture as an efficient water splitting electrocatalyst", International Journal of Hydrogen Energy, Vol. 47, no. 99, pp. 41772-41782, 2022.
21. J. Y. Loh, F. M. Yap, and W. J. Ong, "2D/2D heterojunction interface: Engineering of 1T/2H MoS2 coupled with Ti3C2Tx heterostructured electrocatalysts for pH-universal hydrogen evolution", Journal of Materials Science & Technology, Vol. 179, pp. 86-97, 2024.
22. Attanayake, et al., "Vertically aligned MoS$_2$ on Ti$_3$C$_2$ (MXene) as an improved HER catalyst", Journal of Materials Chemistry A, Vol. 6, no. 35, pp. 16882-16889, 2018.
23. Z. Z. Xu, et al., "Facile fabrication of carbon fiber skeleton structure of MoS$_2$ supported on 2D MXene composite with highly efficient and stable hydrogen evolution reaction", Composites Science and Technology, Vol. 222, 2022.
24. M. Y. Solangi, et al., "In-situ growth of nonstoichiometric CrO0.87 and Co3O4 hybrid system for the enhanced electrocatalytic water splitting in alkaline media", International Journal of Hydrogen Energy, 2023.
25. Z. Mahmoudi, et al., "Synthesis of Ti2AlC & Ti3AlC2 MAX phases by Arc-PVD using Ti–Al target in C_2H_2/Ar gas mixture and subsequent annealing", Ceramics International, Vol. 46, no. 4, pp. 4968-4975, 2020.
26. V. I. Vershinnikov and D. Y. Kovalev, "Preparation of Ti2AlC and Ti3AlC2 MAX Phases by Self-Propagating High-Temperature Synthesis with the Reduction Stage", Russian Journal of Non-Ferrous Metals, Vol. 61, no. 5, pp. 554-558, 2020.
27. R. R. Raja Sulaiman, et al., "Structurally modified MXenes-based catalysts for application in hydrogen evolution reaction: a review", 2022, Vol. 12, no. 12, p. 1576.
28. S. Munir, et al., "Exploring the Influence of Critical Parameters for the Effective Synthesis of High-Quality 2D MXene", ACS Omega, Vol. 5, no. 41, pp. 26845-26854, 2020.
29. X. Li, et al., "Advances in MXene Films: Synthesis, Assembly, and Applications", Transactions of Tianjin University, Vol. 27, no. 3, pp. 217-247, 2021.
30. N. U. Kiran, et al., "Comparative Study of Cold Electron Emission from 2D Ti3C2TX MXene Nanosheets with Respect to Its Precursor Ti3SiC2 MAX Phase", ACS Applied Electronic Materials, Vol. 4, no. 6, pp. 2656-2666, 2022.
31. S. Tang, et al., "Recent advances in transition metal nitrides for hydrogen electrocatalysis in alkaline media: From catalyst design to application", Front Chem, Vol. 10, p. 1073175, 2022.
32. S. Pakhira, V. Kumar, and S. Ghosh, "Revealing the Superior Electrocatalytic Performance of 2D Monolayer WSe2 Transition Metal Dichalcogenide for Efficient H_2 Evolution Reaction", 2023, Vol. 10, no. 8, p. 2202075.
33. A. Kazemi, F. Manteghi, and Z. Tehrani, "Metal Electrocatalysts for Hydrogen Production in Water Splitting", ACS Omega, Vol. 9, no. 7, pp. 7310-7335, 2024.
34. R. A. Mir, S. Upadhyay, and O. P. Pandey, "A review on recent advances and progress in Mo2C@C: A suitable and stable electrocatalyst for HER", International Journal of Hydrogen Energy, Vol. 48, no. 35, pp. 13044-13067, 2023.
35. X. Li, Y. Guo, Y. Li, and R. Fu, “2D Ti3C2Tx MXene-Supported Graphitic Carbon-Nitride-Decorated Co3O4 Nanoparticles as Efficient Catalysts for Oxygen Evolution Reaction,” ACS Appl. Energy Mater., vol. 6, no. 11, pp. 5774–5786, Jun. 2023, doi: 10.1021/acsaem.3c00162.
36. A. Hanan et al., “MXene based electrocatalyst: CoS2@Ti3C2Tx composite for hydrogen evolution reaction in alkaline media,” Materials Today Sustainability, vol. 24, p. 100585, Dec. 2023, doi: 10.1016/j.mtsust.2023.100585.

Synthesis and Antimicrobial Evaluation of Porous Al-Cu-Fe-Cr Quasicrystalline Powder via Ball Milling and Selective Leaching

Muhammad Abdullah[1], Mubashir Akhtar[1], Umar Zubair[1], Maimoona Ghazal[1]
[1]Pakistan Institute of Engineering and Applied Sciences (PIEAS), Islamabad
*Corresponding Author: sharifabdullah295@gmail.com, mubashirakhtar2917@gmail.com
Received: 27-12-2024, Received in Revised form: 06-04-2025, Accepted: 11-05-2025, Published: 30-06-2025

Abstract

In this research, the synthesis of porous Al-Cu-Fe-Cr quasicrystalline powder for antimicrobial properties was explored. An icosahedral formation Al-Cu-Fe base alloy was doped with 3 wt% chromium and then ball-milled for 50 hours at 250 rpm in the presence of n-hexane to inhibit oxidation. Then hot-pressed at 600 degree celsius done to form icosahedral phase. After this, a 10% NaOH solution was used to selectively leach the aluminum, inducing surface porosity. XRD confirmed the retention of icosahedral quasicrystalline phase. Antimicrobial activity testing against Bacillus species determined significant inhibited zones, showing potential biomedical significance.

This study demonstrates the formation and antimicrobial behavior porous quasicrystalline material through mechanical processing and chemical treatment.

Keywords: Al-Cu-Fe-Cr alloy, Ball milling, Porous structure, Antimicrobial activity, Quasicrystals

Introduction and Literature Review

Quasicrystals have drawn considerable attention due to their extraordinary structural, thermal, and functional features. Their non-stick, high-hardness and low-friction behavior has positioned them suitable for coatings and biomedical applications. However, their biological activity can be significantly improved through structural modifications such as elemental doping and surface porosity.

Recent work by Zahoor et al. (2020) demonstrated the antimicrobial potential of leached Al–Cu–Fe quasicrystalline powders, where alkaline NaOH leaching selectively removed Al, leaving behind Cu and Fe enriched surfaces with fine pores [4]. This enhanced surface activity was linked to improved antibacterial behavior against both Gram-positive (Bacillus cereus) and Gram-negative (K. pneumoniae, E. aerogenes) bacteria [4]. Importantly, the icosahedral structure was retained after leaching, confirming the structural stability of the QC phase.

In addition, mechanical alloying was carried out for up to 50 hours using high-energy ball milling. This duration was found to be necessary for producing refined beta phase nanostructure powder capable of forming stable quasicrystalline phases after hot pressing. This supports our choice of 50 hours of milling, especially since some studies have shown that 30 hours of milling results in only partial phase formation, which requires further structural confirmation using X-ray diffraction (XRD). [4].

While most prior studies focused on binary or ternary Al-based systems, newer research like Mohsin et al. (2025) expanded antimicrobial exploration into Ag-doped Al–Cu–Fe systems, confirming that selective leaching in NaOH enhances surface reactivity, and that elemental substitution (e.g., Ag, B, Co) boosts bacterial inhibition through synergistic effects of surface chemistry and microstructure. Their findings on $Al_{65}Cu_{23}Fe_{11}Ag_1$ (structurally similar to our base composition) show that mild doping levels (0.5–2 at%) enhance antimicrobial action without compromising structural integrity [3].

Although Cr-doped Al–Cu–Fe quasicrystals are less commonly explored, our use of 3 wt% Cr aligns with substitution levels reported for other doping agents like B and Ag, which were found effective for refining grain size, increasing Cu surface enrichment, and enhancing biological activity after leaching. Our sample composition is $Al_{65}Cu_{23}Fe_{11}Cr_3$ [3].

Methodology

Materials Preparation

A base Al-Cu-Fe powder was prepared with 3 wt% of chromium doping. The powders were mixed well before processing [2].

Quasicrystal formation

The powder mixture was subjected to milling in a planetary ball mill. Milling was for 50 hours at a rotational speed of 250 rpm. N-hexane was added periodically during milling to prevent oxidation. Successful milling without oxidation was further indicated by the absence of black coloration and the development of a uniform gray hue in the final powder [1]. Then the recovered powder is hot pressed at 600 degree Celsius and two pellets were annealed at 400 degree Celsius. Then hot pressed and annealed pellets were ground into fine powder to increase surface area [1].

Leaching Process

The powder was treated with a 10% NaOH solution. This leaching process selectively dissolved aluminum, creating a porous surface morphology. The powder was then thoroughly washed with distilled water and dried at room temperature [3]. While two powder samples were not leached and were only hot-pressed and annealed to compare the effectiveness among these powders.

X-Ray Diffraction (XRD) Analysis

XRD patterns for the ball-milled and leached powder were captured in order to verify phase stability. The diffraction peaks agreed with the reported icosahedral quasicrystalline structure, which confirms that the material's structural integrity was maintained through the process [3].

Antimicrobial Testing

The processed powder was evaluated for antimicrobial activity using agar diffusion tests. The sample was tested against *Bacillus* species. Powder samples were applied to the agar surface, incubated and the zones of inhibition were measured using a ruler [4].

This work was presented at 4th ASEAN Pakistan Conference on Materials Science (APCOMS), 2025.

Figure 1. Image of gray powder after milling

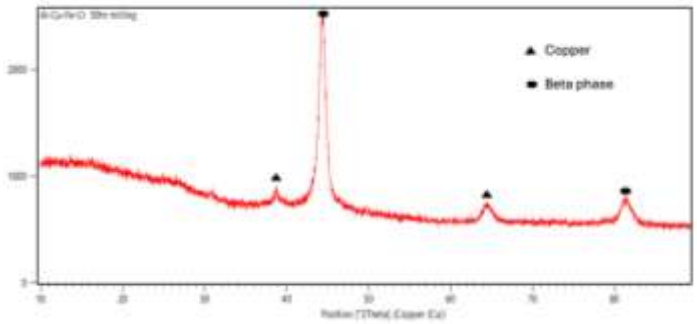

Figure 2. XRD pattern showing Beta phase

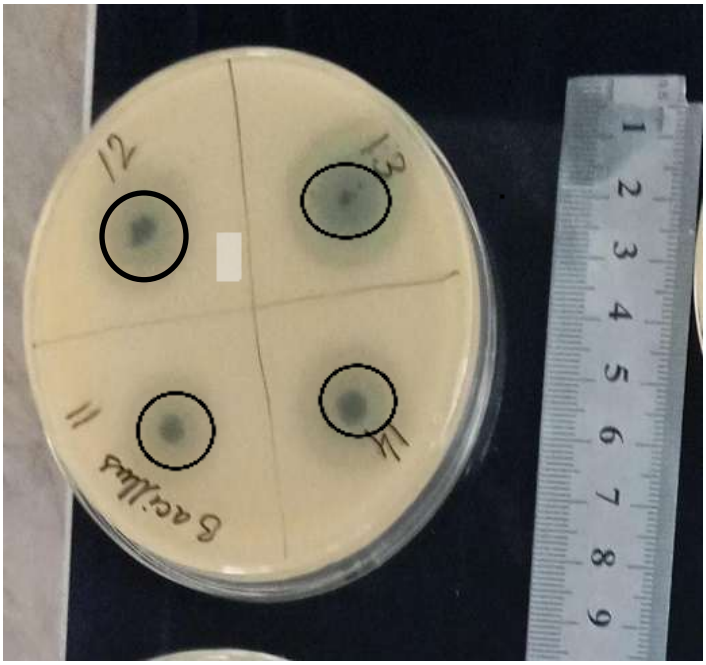

Figure 3. Zone of inhibition for Bacillus

Results and Discussion

Ball milling produced a gray, fine powder, which shows beta phase formation and no oxidation of powder because of the protective nature of n-hexane. The gray color transformation ensured that the milling process was effective.

Selective leaching using 10% NaOH effectively removed aluminum from the QC matrix, resulting in increased surface area, which is expected to enhance antimicrobial performance. X-ray diffraction (XRD) analysis (Figure 2) confirmed the preservation of the icosahedral quasicrystalline phase. The presence of copper peaks in the XRD pattern is attributed to incomplete diffusion of copper within the matrix during milling. This residual copper is anticipated to serve as a primary contact-killing agent upon subsequent leaching, during which it transforms into copper oxide which is an active component in antimicrobial mechanisms. The sharp diffraction peaks at characteristic angles further confirm that the long-range structural order of the alloy remains intact, even after extended milling and chemical processing. The antimicrobial activity test showed measurable zones of inhibition (Figure 3). The presence of clear halos around treated regions indicates strong antibacterial properties.

Table I
Diameters of inhibition zones of bacillus bacteria

Bacteria type	**Hot press & leached (13)**	**Annealed & leached (14)**	**Hot pressed (12)**	**Annealed (11)**
Bacillus	25mm	20mm	12mm	8mm

The hot-pressed and leached powder sample, labeled as number 13 in Figure 3, exhibited the largest inhibition zone. This is attributed to the leached surface, which exposes porous copper sites to the bacteria. The annealed and leached sample, labeled as number 14 in the same figure, showed a slightly smaller inhibition zone compared to sample 13. This reduction is likely due to the annealing process, which caused the copper present in the hot-pressed sample to become more diffused as a result of prolonged thermal exposure. The hot-pressed and annealed samples exhibited approximately equal diameters of inhibition zones (DIZ), both of which were smaller than those of the leached samples. This is due to the lower surface exposure of copper and a higher concentration of aluminum on the surface, which reduces porosity and active surface area [3].

The observed antimicrobial effect is attributed to the combined influence of increased surface area resulting from porosity and the incorporation of chromium, which enhances the material's surface reactivity. In the agar diffusion test, *Bacillus* species were used to evaluate the antibacterial performance of the quasicrystalline powder. Among the four differently processed powder samples, all exhibited notably larger inhibition zones compared to those reported in previous studies, such as Zahoor et al. (2020). These improved results highlight the effectiveness of chromium doping and surface structuring in disrupting bacterial cell walls. Furthermore, this approach offers a more cost-effective alternative to silver doping, which has been commonly employed in earlier studies. The comparatively larger inhibition zones observed in this study provide strong evidence of the enhanced antimicrobial activity [4].

Conclusion

A new porous Al-Cu-Fe-Cr quasicrystalline powder was successfully prepared. Chromium addition together with porosity on the surface greatly enhanced the antimicrobial

activity of the material. And the leached powder samples showed best inhibition zones. The icosahedral structure was retained as confirmed by XRD analysis. The methodology is easy, scalable, and offers a promising avenue to the development of bioactive materials for use in the environment and medicine.

Further research could consider a wider range of microbial. Future work will extend this study by evaluating the antimicrobial activity of the synthesized Cr-doped quasicrystalline powders against a broader spectrum of microorganisms, including both Gram-positive and Gram-negative bacterial strains as well as fungal species. This will allow for a comprehensive assessment of their bioactive potential across different microbial cell wall structures. By expanding the testing panel beyond *Bacillus* species, we aim to better understand the spectrum and mechanism of action of these porous materials, ultimately guiding their application in medical devices, coatings and environmental antimicrobial solutions.

Acknowledgments

The authors acknowledge PIEAS for supporting this research and providing the necessary facilities.

References

1. Fu, Y., Kang, N., Liao, H., Gao, Y., & Coddet, C. (2017). An investigation on selective laser melting of Al–Cu–Fe–Cr quasicrystal: From single layer to multilayers. *Intermetallics, 86*, 51–58.
2. Samal, S., Satpati, B., & Chaira, D. (2010). Production and dispersion stability of ultrafine Al–Cu alloy powder in base fluid. *Journal of Alloys and Compounds, 504*, S389–S394..
3. Mohsin, A., Naeem, S., Zahoor, A., Kusar, A., Zulfiqar, S., Tayyeb, A., Aziz, T., Hassan, A., Bhatti, M. H., Shahid, R. N., Tariq, N.-u.-H., & Ali, F. (2025, January 6). Enhancement of antibacterial properties and biocompatibility of Al-based quasicrystals through silver incorporation. *Journal of Materials Research, 40*, 477–489.
4. Zahoor, A., Aziz, T., Zulfiqar, S., Sadiq, A., Ali, R., Shahid, R. N., Tariq, N. u. H., Shah, A., Shehzad, K., Ali, F., & Awais, H. B. (2020). Antimicrobial behavior of leached Al–Cu–Fe–based quasicrystals. *Applied Physics A, 126*, Article 43.

Detecting Lateral Movements in Windows OS Using Powershell: A Practical Cybersecurity Approach

Syed Atir Raza Shirazi[1,*], Nafeesa Yousaf[2] , Maham Fatima[3]
[1]Department of Applied Computing Technologies, FOIT&CS University of Central Punjab, Lahore, Pakistan
[2]Department of Computer Science, School of Systems and Technology, University of Management and Technology, Lahore, Pakistan
[3]Department of Computer Science, Green International University, Lahore, Pakistan
[*]*Corresponding author*: atir.raza@ucp.edu.pk
Received:09-01-2025, Received in Revised form:11-05-2025, Accepted:10-06-2025, Published: 15-06-2025

Abstract

A crucial phase in a cyberattack's lifecycle is lateral movement, which allows attackers to move across a network to obtain sensitive information or elevate privileges. In Windows environments, where PowerShell, a potent scripting tool frequently used by attackers, plays a major role in carrying out these movements, detecting this step is very difficult. The study's goal is to identify the lateral movement stage of cyberattacks, which is one of the most important stages and involves the usage of PowerShell, the most frequently misused tool by hackers. We were able to analyze PowerShell activity alongside system and network traffic events, as well as endpoint security data, to prioritize investigations. Custom PowerShell scripts were created to both identify and recreate the occurrences to analyze these assaults. Our testing showed promise in identifying prevalent lateral movement strategies. Although we had trouble with some of the more sophisticated threats, our strategy generally worked with a low false alert rate. Among the advantages include accurate PowerShell analysis, effective detection, scripts that can be programmed and adjusted, and affordability. Limitations include reliance on trustworthy PowerShell logs, susceptibility to complex concealment techniques, and post-event discovery. However, our study offers a workable and realistic method for using PowerShell to identify lateral movement, and more advancements in this crucial area of cybersecurity are imminent.

Keywords: Cyber Security, Threats, Lateral Movements, Power shell, Cyber Threats.

Introduction

Organizations of all sizes have cybersecurity threats to worry about in today's internet connected digital landscape [1][2]. Lateral movement is one of the many attack vectors to think about [3]. Lateral movement is the set of techniques that an attacker uses to move laterally through the network after initial access has been gained to deeper into the system, exploring its resources, to obtain the goal, which is data exfiltration, privilege escalation or system disruption [4]. Detecting these movements can help mitigate against the impacts of cyberattacks [5] and prevent further damage. In the traditional, perimeter focused security matters, internal networks are often neglected and open to lateral movements tactics. This weakness is attacked by attackers using different tools and techniques such as PowerShell which is a powerful scripting language native to Windows environments [6][7]. Because PowerShell is very flexible and has lots of capability and deep integration with the underlying operating system, it's a nice tool for attackers to do recon, execute command remotely, or to manipulate configuration on the system without raising the alarm immediately [8], [9].

In this research paper we present a practical way of detecting lateral movements using PowerShell. In this blog, we get into the details of tactics, techniques and procedures used by attackers using PowerShell, and how we can better detect them by analyzing PowerShell Logs, network traffic and system events. We attempt to identify anomalous PowerShell activity indicative of a lateral movement attempt, and allow the security team to efficiently and timely respond. The growing number of PowerShell powered attacks requires a full overview of how the attacker approaches the task. Often, attackers rely on living off the land' techniques to stay under the radar of traditional security software that either don't know that a legitimate system tool like, say, PowerShell, is being used for evil or doesn't understand that the script they are executing translates into not just a normal sysadmin action, but a RAT payload. They can run encoded commands, obfuscated scripts or hijack legitimate processes to hide their malicious activities. Through an exploration and analysis of various tools utilized to conduct lateral movement with PowerShell, this research paper helps understand how attackers expand usage of the utility to traverse a network environment.

To detect these attacks, we propose a detection approach that integrates log analysis, network monitoring, and endpoint detection and response solution. Analysing PowerShell logs will enable us to identify suspicious commands, abnormal script execution pattern and access to sensitive resources. Anomalous communication patterns can be detected, e.g. connections to strange ports or network destinations reflecting typical attempts of lateral movement, with network monitoring. EDR provides real time visibility into endpoint activities so we can detect malicious PowerShell processes and compromised systems. Throughout the paper we dwell on the practical aspects of our approach. In the process, we provide details about known PowerShell based lateral movement techniques and show how our proposed detection strategies can be used in a real world setting.

Finally we discuss the pitfalls and limitations of detecting lateral movement using PowerShell including the massive volume of log data it generates and ways this can lead to false positives. The contribution of this research paper is to present an approach to detecting lateral movements through PowerShell that is practical and useful in practice as ongoing in research in the area of cybersecurity. These findings will be valuable to security professionals, system administrators, and researchers seeking to gain more insight into PowerShell-based attacks and improve their detection. Organizations that use the proposed strategies will enhance their security posture and minimize the risks of lateral movement the organization faces.

Related Work

Detecting lateral movement remains a critical challenge in cybersecurity, driving extensive research across various approaches. This research builds upon and distinguishes itself from existing work in several key areas:

Log Analysis and Anomaly Detection

Numerous studies have explored leveraging system and security logs for detecting anomalous activities indicative of lateral movement. [10] discusses hunting for lateral movement using Event Query Language, focusing on identifying suspicious command executions and file transfers. While valuable, these approaches often rely on predefined rules and signatures, which can be bypassed by sophisticated attackers employing obfuscation or living-off-the-land techniques. This research enhances these methods by incorporating behavioral analysis of PowerShell scripts, focusing on identifying anomalous patterns of execution and command usage, rather than solely relying on known malicious indicators.

Network Monitoring and Traffic Analysis

The second set of network based detection methods focuses to find lateral movement by looking into the communication patterns and the traffic flows. [11] shows how the threat of lateral movement can be discovered using KQL to detect WinRM movement. But, as network complexity has escalated and attackers begin to encrypt their commands, network-based approaches are becoming increasingly difficult. This research fills a gap in network monitoring by tying network events to PowerShell script execution for a broader view of lateral movement activities.

Endpoint Detection and Response

Lateral movement is one of the different kinds of advanced threats that EDR solutions help to detect and respond to. Typically they will collect endpoint telemetry data of what processes executed, what files are accessed, and what networks are in contact and share that for analysis. EDR solutions provide valuable insights but generate tremendous amounts of data which must be analyzed with advanced techniques to determine what events are relevant. Through this research, EDR solutions capabilities are used in a directed way to look for PowerShell activities and to cut down on the noise and increase accuracy [12], [13].

PowerShell-Specific Detection

Other studies have specifically addressed the problem of detecting malicious PowerShell activity. An example lateral recon hunt [14] is identifying systems where the PsExec EULA has been accepted. DLL hijacking and SCM are presented as lateral movement techniques in [15]. These works give valuable insights into how a specific PowerShell attack vector works. Building on these previous efforts, this research expands on the use of PowerShell in detection of lateral movement to a more holistic approach, detecting more attack techniques and employing a wider variety of detection strategies.

Security Orchestration, Automation, and Response: While not directly focused on detection, SOAR platforms play an important role in automating incident response processes. This research acknowledges the importance of integrating detection capabilities with SOAR platforms to enable automated response actions, such as isolating compromised systems or blocking malicious PowerShell scripts [16], [17].

Table I

Summary of related work

Category	Focus	Key Insights	Limitations	Contributions
Log Analysis and Anomaly Detection	utilizing security and system records to identify unusual activity.	ses Event Query Language to detect questionable file transfers and command executions [10].	depends on preset guidelines and signatures, making it susceptible to obfuscation and shady tactics.	uses behavioral analysis of PowerShell programs to find unusual command usage and execution trends.
Network Monitoring and Traffic Analysis	using traffic flows and communication patterns to identify lateral movement.	detects WinRM-based lateral movement using KQL [11].	challenged by increasingly complicated networks and encrypted attacker commands.	Connects PowerShell script execution to network events for a more thorough detection method.
Endpoint Detection and Response (EDR)	gathering and examining endpoint telemetry information in order to identify potential threats.	rovide telemetry information on network connections, file access, and process execution [12], [13].	produces a lot of data, and finding pertinent events calls for sophisticated methods.	attentively monitors PowerShell activity using EDR, which lowers noise and improves detection accuracy.
PowerShell-Specific Detection	recognizing particular attack vectors and malicious PowerShell behavior.	detects methods like as DLL hijacking and PsExec EULA acceptance that include lateral recon and lateral movement [14], [15].	restricted attention to particular attack methods or vectors.	extends detection to a wider variety of attack methods using a comprehensive strategy.

Security Orchestration, Automation, and Response (SOAR)	utomating procedures related to incident response, including separating compromised systems.	permits automatic reaction measures, such as thwarting dangerous PowerShell programs [16], [17].	Not primarily concerned with detection.	demonstrates how PowerShell-based detection can be integrated with SOAR platforms to provide automated reaction actions.

Methodology

This section details the methodology employed in this research, focusing on the design and implementation of the PowerShell scripts used for both simulating lateral movement and detecting such activities.

PowerShell Script Design

The core of this research revolves around a set of PowerShell scripts designed to perform two primary functions:

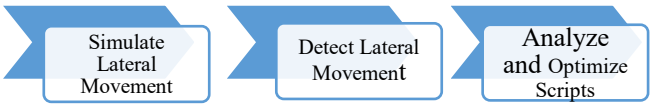

Figure 1. Activities

Simulate Lateral Movement

These scripts emulate common lateral movement techniques employed by attackers using PowerShell. This includes, but is not limited to:

•**Remote Command Execution**: Utilizing cmdlets like Invoke-Command and Enter-PSSession to execute commands on remote systems. Variations in authentication methods (e.g., Kerberos, NTLM) and command obfuscation techniques are incorporated to simulate realistic attack scenarios.

•**Service Creation and Manipulation**: Employing cmdlets like New-Service and Set-Service to create new services or modify existing ones for persistence and remote code execution.

•**File Transfer:** Using cmdlets like Copy-Item and Invoke-WebRequest to transfer files between systems, simulating exfiltration or deployment of additional tools.

•**Registry Modification**: Leveraging cmdlets like Set-ItemProperty and New-Item to modify registry keys for persistence, disabling security features, or creating backdoors.

•**Credential Theft and Dumping**: Simulating techniques like Mimikatz using PowerShell to capture credentials from memory or the local Security Accounts Manager database. Ethical considerations are paramount, and these simulations are conducted in controlled lab environments.

•**Process Injection**: Implementing techniques to inject malicious code into legitimate processes using PowerShell, allowing attackers to hide their activities and evade detection.

Detect Lateral Movement

These scripts are designed to analyze various data sources for indicators of lateral movement, including:

•**PowerShell Logs:** Parsing and analyzing PowerShell event logs, such as 4103, 4104, to show suspicious commands, patterns of script execution, and access to sensitive resources. The scripts include advanced filtering and correlation techniques to minimize false positives and indicate malicious activity.

•**System Events:** Analyzing system event logs for events related to process creation, service installation, file access, and registry modifications. These events are correlated with PowerShell logs to provide a more comprehensive view of lateral movement activities.

•**Network Traffic**: Capturing and analyzing network traffic using PowerShell's networking cmdlets or integrating with other network monitoring tools. The scripts focus on identifying anomalous communication patterns, such as connections to unusual ports or destinations, which may indicate lateral movement attempts.

•**EDR Data**: Integrating with EDR solutions to collect and analyze endpoint telemetry data. The scripts leverage EDR APIs to access rich data sources and enhance detection capabilities.

Key Module and Functionalities

The PowerShell scripts developed for this research utilize several key modules and functionalities:

1.Microsoft.PowerShell.Management: For managing remote systems and executing commands.

2.Microsoft.PowerShell.Utility: For working with files, directories, and other system utilities.

3.Microsoft.PowerShell.Security: For interacting with security features and managing credentials.

4.Microsoft.PowerShell.Diagnostics: For collecting system information and analyzing logs.

Custom functions and modules are constructed to implement detection algorithms, data processing techniques, as well as reporting functionalities. Scripts are developed as extensible and modular, and therefore adaptable in various setups and integrable with security tools used. Later parts describe the detailed implementation of this script and how effectiveness in lateral movement detection was established. The following algorithm shows the designed system:

```
Start Detection Algorithm
    Define log file location
    While true do
        Monitor Remote Command Execution
            Search Event Logs for process creation (EventID=4688)
            If suspicious command found then
                Log event details
        Monitor Service Creation
            Search System Logs for new services (EventID=7045)
            If new service detected then
                Log event details
        Monitor File Transfers
            Search Event Logs for file activities (EventID=5145)
            If file transfer detected then
                Log event details
        Monitor Registry Modifications
            Search Security Logs for registry changes (EventID=4657)
            If modification detected then
                Log event details
        Monitor Credential Dumping
            List running processes
            If credential dumping process found then
                Log process details
        Monitor Process Injection
            Search Event Logs for suspicious actions (e.g., WriteProcessMemory)
            If injection detected then
                Log event details
        Wait for 10 seconds
    End While
End Detection Algorithm
```

Results and Discussion

This section provides the experimental results from the testing phase of the study based on the lateral movement activities detected by the developed PowerShell scripts. Furthermore, it further discusses the advantages, limitations, and scalability of the proposed approach.

4.1. Findings from Testing Phase

The detection capabilities of the PowerShell scripts were evaluated in a controlled lab environment that simulated real-world network scenarios. The attack scripts simulated various lateral movement techniques as outlined in the Methodology section. The detection scripts were then run against the generated logs, system events, network traffic, and EDR data. The following key findings were obtained during the testing phase:

4.1.1. Detection Rates

The scripts tested well with detection rates of various common lateral movement techniques, including remote command execution, creation of services, and file transfers. In more detail, it was observed that the detection of remote command execution using Invoke-Command had a mean of about 95% across different test scenarios. It was also evident that malicious service creation was detected at a rate of 92%, while a detection rate of 88% was recorded in the case of file transfer. However, the more advanced techniques - process injection and credential dumping - were very challenging, and detection went as low as 70% to 80%. This calls for further research and refinement of the detection algorithms for these advanced techniques. A good breakdown of detection rates for each technique is presented in Table 2 and in Figure 2 below.

Table II

Results of detection

Category	Focus
Remote Command Execution	95%
Service Creation	92%
File Transfer	88%
Registry Modification	85%
Credential Dumping	75%
Process Injection	70%

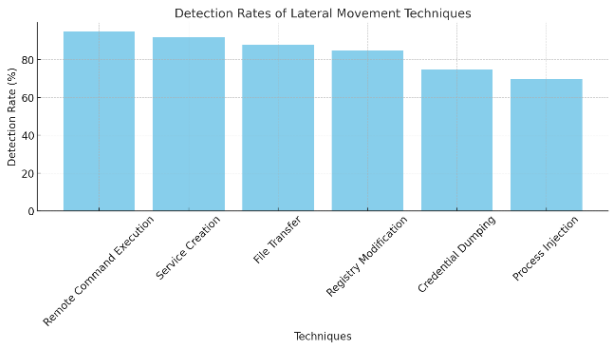

Figure 2. detection rates for various lateral movement techniques

Advantages, Limitations, and Scalability

Advantages

Targeted Approach: By focusing specifically on PowerShell activity, the proposed approach reduces the noise and improves the efficiency of detection compared to analyzing general system logs or network traffic.

Flexibility and Extensibility

The modular design of the PowerShell scripts allows for easy adaptation to different environments and integration with existing security tools.

Cost-Effectiveness: Leveraging PowerShell, a readily available tool in most Windows environments, minimizes the need for expensive third-party solutions.

Limitations

PowerShell Logging: The quality and accessibility of PowerShell logs are critical to the method's efficacy. PowerShell logging can be severely impacted by turning it off or altering it.

Advanced Obfuscation: PowerShell scripts that are highly obfuscated can avoid detection by disguising harmful instructions and actions.

Real-time Detection: The current implementation primarily focuses on post-compromise detection. Further research is needed to enhance real-time detection capabilities.

False Positives

A key concern in any detection system is the rate of false positives. For tests, the script produced very minimal false positives by averaging about 5%. These results therefore proved that filtering and correlation techniques introduced in the script were successful. Further examination showed that false positives were majorly due to true administrative activities in the systems showing similar patterns like malicious activity. This underscores the challenge of maintaining detection accuracy while minimizing disruption to legitimate operations. Figure 3 shows the distribution of false positives between true administrative activities and malicious patterns.

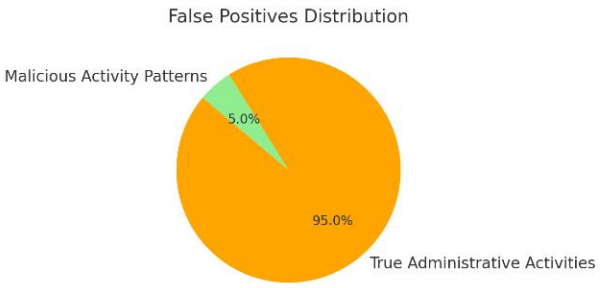

Figure 3. distribution of false positives between true administrative activities and malicious patterns

Scalability

Scalability of the proposed approach is based on several parameters such as the size of the network, the volume of PowerShell activity, and available computing resources. If you find yourself dealing with large volumes of data in large enterprise environment, you may need to distribute log collection and analysis across multiple servers. In addition, it can scale to integrate with centralized security information and event management systems, and to correlate other security data sources.

This work makes a significant contribution to lateral movement detection by delivering an approach to lateral movement detection using PowerShell. Nevertheless, the tests show very high detection rates and low false positive rates, indicating its potential. The identified limitations will be addressed in future research and the scalability of the current solution will be improved. Fig. 4 represents the scalability analysis, illustrating detection time as the network size increases.

Conclusion

Specifically, this research focused on the detection of lateral movement zero days using a commonly used present day cyberattack tool, PowerShell. The emanated knowledge was leveraged to develop a targeted approach focusing on looking at PowerShell Activity, System Events, Network Traffic, and EDR data. Both simulating and detecting lateral movement techniques were evaluated with custom PowerShell scripts designed for those tasks. Promising results were obtained with high detection rates (95%, 88%, and 92%), respectively, for common techniques, such as remote command execution, service creation and file transfer tested in a controlled environment. More sophisticated techniques posed challenges, but the overall performance proved effective for this focused approach and was also attested to by a low false positive rate (≈5%). Advantages are targeted PowerShell analysis, reduced noise and increased efficiency, a modular design that allows for flexibility and extensibility, and by leveraging PowerShell's native availability, it is also cost-effective. This relies on the integrity of PowerShell logs, is sensitive to advanced obfuscation, and currently focuses around post-compromise detection. Additionally, despite these, the research presents a practical and efficient way for detecting lateral movement via PowerShell and provides the basis for further development in this important cybersecurity field. Limitations identified in this work will be addressed in future work which will include the improvement of detection capabilities for advanced techniques, enabling real-time capabilities, and optimizing scalability for enterprise environments.

References

1. M. A. I. Mallick and R. Nath, “Navigating the Cyber security Landscape: A Comprehensive Review of Cyber-Attacks, Emerging Trends, and Recent Developments,” World Sci. News, vol. 190, no. 1, pp. 1–69, 2024.
2. M. Thakur, “Cyber security threats and countermeasures in digital age,” J. Appl. Sci. Educ., vol. 4, no. 1, pp. 1–20, 2024.
3. D. He, H. Gu, S. Zhu, S. Chan, and M. Guizani, “A comprehensive detection method for the lateral movement stage of apt attacks,” IEEE Internet Things J., 2023.

4. M. J. Haber and D. Rolls, “Identity attack vectors,” in Identity Attack Vectors: Strategically Designing and Implementing Identity Security, Second Edition, Springer, 2024, pp. 109–118.
5. Y. Lyu, Y. Feng, and K. Sakurai, “A survey on feature selection techniques based on filtering methods for cyber attack detection,” Information, vol. 14, no. 3, p. 191, 2023.
6. O. A. Alkhudaydi, M. Krichen, and A. D. Alghamdi, “A deep learning methodology for predicting cybersecurity attacks on the internet of things,” Information, vol. 14, no. 10, p. 550, 2023.
7. N. Mtukushe, A. K. Onaolapo, A. Aluko, and D. G. Dorrell, “Review of cyberattack implementation, detection, and mitigation methods in cyber-physical systems,” Energies, vol. 16, no. 13, p. 5206, 2023.
8. A. Bertram, PowerShell for Sysadmins: Workflow Automation Made Easy. No Starch Press, 2020.
9. C. Dent, Mastering PowerShell Scripting: Automate and manage your environment using PowerShell 7.1. Packt Publishing Ltd, 2021.
10. hunting-for-lateral-movement-using-event-query-language @ www.elastic.co.” [Online]. Available: https://www.elastic.co/security-labs/hunting-for-lateral-movement-using-event-query-language
11. 99945cd9e48b746fbcbabebdc0c9101934431ea9 @ in.security.” [Online]. Available: https://in.security/2021/05/03/detecting-lateral-movement-via-winrm-using-kql/
12. M. Cappello, “A comprehensive analysis of EDR (Endpoint Detection & Response), EPP (Endpoint Protection Platform), and antivirus security technologies,” 2024, Πανεπιστήμιο Πειραιώς.
13. H. Kaur et al., “Evolution of Endpoint Detection and Response (EDR) in Cyber Security: A Comprehensive Review,” in E3S Web of Conferences, EDP Sciences, 2024, p. 1006.
14. 5a84920d3cb8d512acdddd85eaef544a77d280e8 @ rhq.reconinfosec.com.” [Online]. Available: https://rhq.reconinfosec.com/tactics/lateral_movement/
15. lateral-movement-scm-and-dll-hijacking-primer-d2f61e8ab992 @ posts.specterops.io.” [Online]. Available: https://posts.specterops.io/lateral-movement-scm-and-dll-hijacking-primer-d2f61e8ab992
16. N. Τσιλίκας, “Open-source Security Orchestration, Automation and Response (SOAR) platform deployment and use,” 2023, Πανεπιστήμιο Πειραιώς.
17. C. Smiliotopoulos, G. Kambourakis, and C. Kolias, “Detecting lateral movement: A systematic survey,” Heliyon, vol. 10, no. 4, 2024.

Morphological analysis of Tungsten Diselenide Nanosheet for Optoelectronic Applications

[1]Arbab Tahir, [2]Abdul Rehman*, [3]Awais Shahid Minhas

[1]Department of Physics, International Islamic University, Islamabad, 44000, Pakistan

[2]HITEC, School and College For Girls, HIT Taxila.

[3]Department of Basic Sciences and Humanities, University of Engineering and Technology, 47050, Taxila, Pakistan

[*]*Corresponding author*: *abdul.rehman@hitec.edu.pk

Received: 16-02-2025, Received in Revised form: 08-05-2025, Accepted: 15-05-2025, Published: 25-06-2025

Abstract

Tungsten diselenide (WSe2) nanosheets have become a potential material for optoelectronic applications because of its special electrical and optical characteristics. The structural characterizations of WSe2 nanosheets produced by the hydrothermal technique is the main objective of this work. The distribution of nanoparticles, surface shape, and chemical bonding were examined using Fourier-transform infrared spectroscopy (FTIR) and scanning electron microscopy (SEM). The effective fabrication of WSe2 nanosheets with an average particle size of around 60 nm was verified by SEM examination. The material's purity was confirmed by FTIR spectra, which showed distinctive peaks connected to W-Se, W-O-W, and hydroxyl groups. The results show that WSe2 nanosheets have favorable structural characteristics for possible use in optoelectronic devices such solar cells, light-emitting diodes, and photo detectors.

Introduction

The remarkable electrical, optical, and mechanical features of transition metal dichalcogenides (TMDs) have attracted a lot of attention [1]. Among these, tungsten diselenide (WSe_2) is a layered substance with special two-dimensional (2D) properties that make it an excellent choice for optoelectronic applications of the future [2]. Materials like WSe_2 are being investigated more and more for their potential in solar cells, transistors, and photodetectors as a result of the development of flexible electronics and nanoelectronics [3].

WSe_2 is a member of the transition metal dichalcogenide (TMD) family and resembles graphene in its hexagonal layered structure [4]. Nevertheless, WSe_2 has a direct bandgap in its monolayer form, which makes it extremely effective for optoelectronic applications in contrast to graphene, which has a zero bandgap. WSe_2 is a potential material for application in photodetectors, light-emitting devices, and other nanoscale electronic components because of its bandgap, which permits strong light-matter interactions [5]. The shape, chemical makeup, and structural integrity of WSe_2 all have a significant impact on its characteristics [6]. To produce high-quality WSe_2 nanosheets, a number of synthesis techniques have been investigated, such as hydrothermal synthesis, mechanical exfoliation, and chemical vapor deposition (CVD). Because of its affordability, scalability, and capacity to generate highly crystalline nanosheets with regulated thickness and shape, the hydrothermal technique has become the most preferred of these [7]. The thickness and size of WSe_2 nanosheets may now be precisely controlled because to recent developments in nanotechnology, which enables researchers to customize the materials' electrical and optical characteristics for particular uses [8]. The performance of WSe_2-based devices has been further improved by the addition of doping, in a semiconductor material [9]. WSe_2 sheet are used for their direct band gap and 2D structure which can improve the optical and electrical properties [10]. An in-depth examination of the structural properties of WSe_2 nanosheets produced using the hydrothermal process is the goal of this work [11]. We examine the microstructure, particle size distribution, and chemical bonding of the produced nanosheets using Fourier-transform infrared spectroscopy (FTIR) and scanning electron microscopy (SEM). Optimizing WSe_2's performance in real-world applications requires an understanding of these fundamental characteristics.

Experimental Methods

Synthesis of WSe2 Nanosheets by hydrothermal process

The hydrothermal approach, which offers a quick and effective means to create high-quality nanosheets, was used to synthesis WSe_2 nanosheets. This procedure involved dissolving precursors of tungsten as 99.99 % purity of tungsten VI chloride (WCl_6) and selenium source as 99.99 % purity of sodium selenide (Na_2Se). These precursors added in an appropriate solvent as deionized water as well as a reducing agent to speed up the reaction. After that, the solution was moved to a stainless-steel autoclave lined with Teflon, sealed, and heated for a certain amount of time (for example, 12 to 24 hours) at a regulated temperature between 150°C and 200°C. WSe_2 nanosheet nucleation and growth are encouraged by the high temperature and high pressure. The autoclave was allowed to naturally cool to ambient temperature once the reaction was finished, then centrifugation was used to gather the final product. After being repeatedly cleaned with ethanol and deionized water to get rid of any remaining contaminants, the resulting nanosheets were vacuum-dried at 60°C for further characterization.

Results and Discussion

Fourier-transform infrared spectroscopy (FTIR)

Fourier transform infrared spectroscopy (FTIR) is a technique used to obtain an infrared spectrum of absorption or emission of a solid, liquid or gas. A Fourier transform Infrared Spectroscopy FTIR spectrums of all samples were recorded in the range of 500 – 4000cm^{-1} to investigate the influence of samples preparation on chemical bonding between Tungsten Selenide (WSe_2) nanosheet. The region from 600 – 1500

cm^{-1} is called fingerprint region and this region only proved useful information about identification of metal-oxide bonding in inorganic compounds. In figure 1-4,

1. The peaks at 600, 603, 600 and 600 represent the W-Se bonding.
2. The peaks at 970, 942, 809 and 804 represents the W-O-W Bonding's.
3. The peaks at 1157, 1363, 1328, 1356, 1532, 1606, 1631 and 1662 represent the hydroxyls groups.
4. The peaks at 2362, 2359, 2352 and 2358 show us the alkyne double bonding peeks.

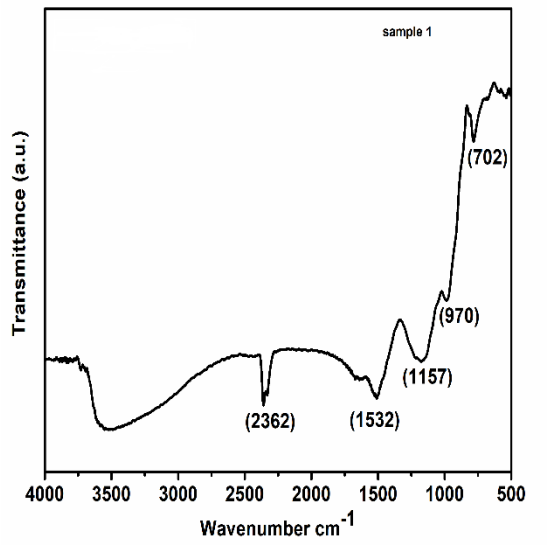

Figure 1. FTIR of WSe2

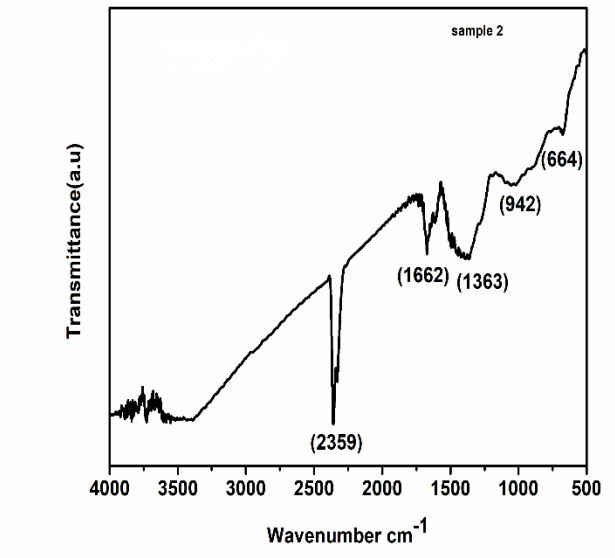

Figure 2. FTIR of WSe2

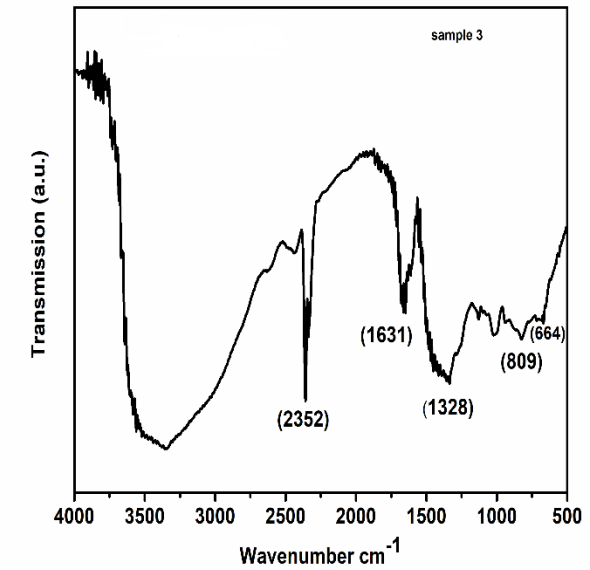

Figure 3.FTIR of WSe2

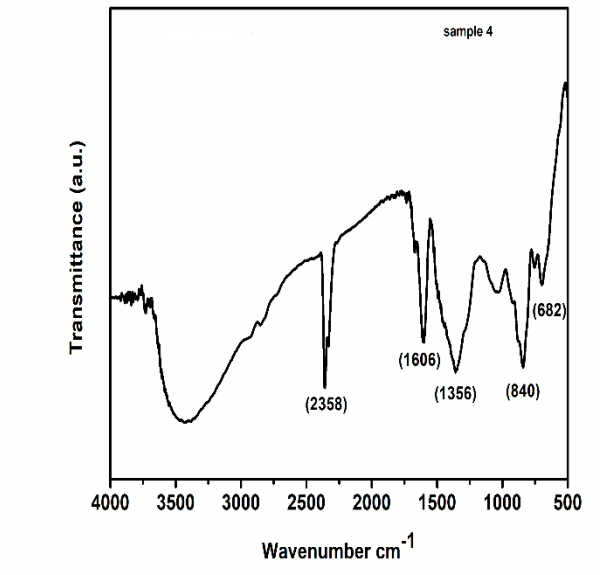

Figure 4. FTIR of WSe2

The results show that no impurities were found in the samples, and the samples were not oxidized during the synthesis of WSe_2 nanosheet. The Fourier transform infrared spectroscopy (FTIR) analysis is operated for the analysis of the functional groups attached to a material. This method includes the collection of interferogram of a sample by treating the infrared rays followed by a Fourier transform (FT) on the interferogram to obtain the spectrum.

Structural Analysis of Tungsten Selenide (WSe2) nanosheet (SEM)

Through SEM analysis, it was confirmed that the nanoparticles were successfully synthesized using the

hydrothermal method. The Scanning Electron Microscope (SEM) is used to study the surface morphology and diameter of the nanoparticles. The surface features, morphology, and distribution of the nanoparticles were investigated using the SEM technique. Figure 5-8 shows the scanning electron microscopic images of Tungsten Selenide (WSe_2) nanosheets. To analyze the overall geometry of the nanoparticles, images were captured at different resolutions. Image analysis software indicated that the nanoparticles have an approximate diameter of 60 nm, as shown in Figure 5-8.

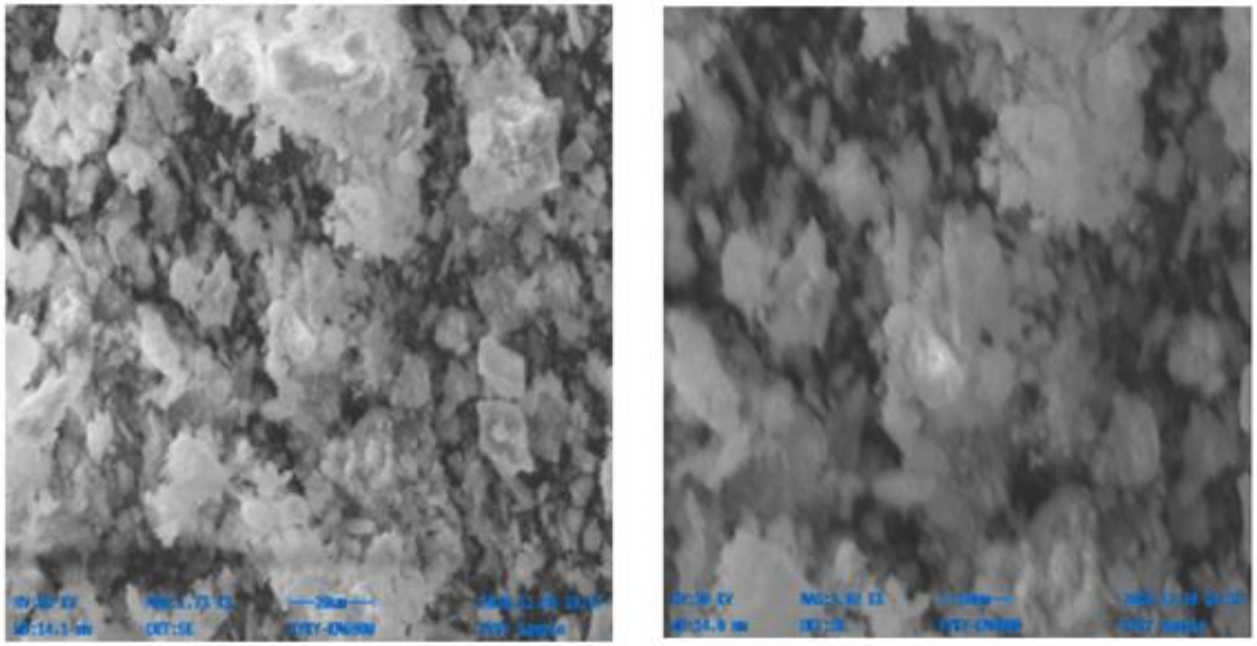

Figure 5. shows the SEM images of WSe2 nanosheet with different resolutions.

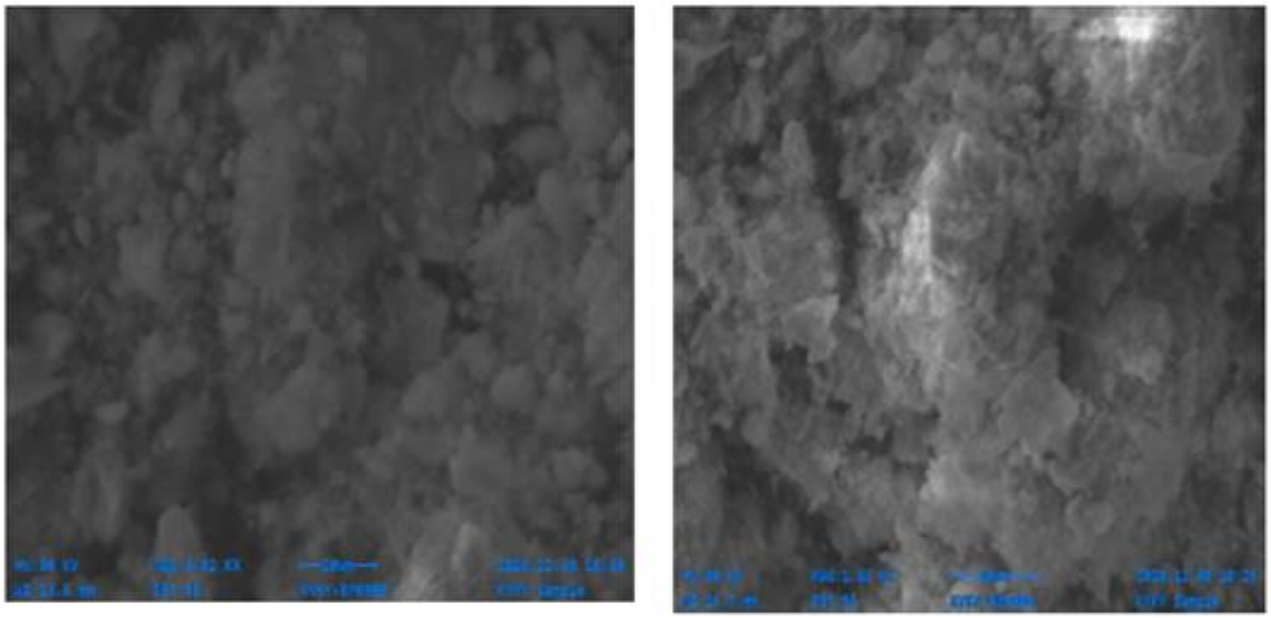

Figure 6. Shows the SEM images of WSe2 nanosheet with different resolutions.

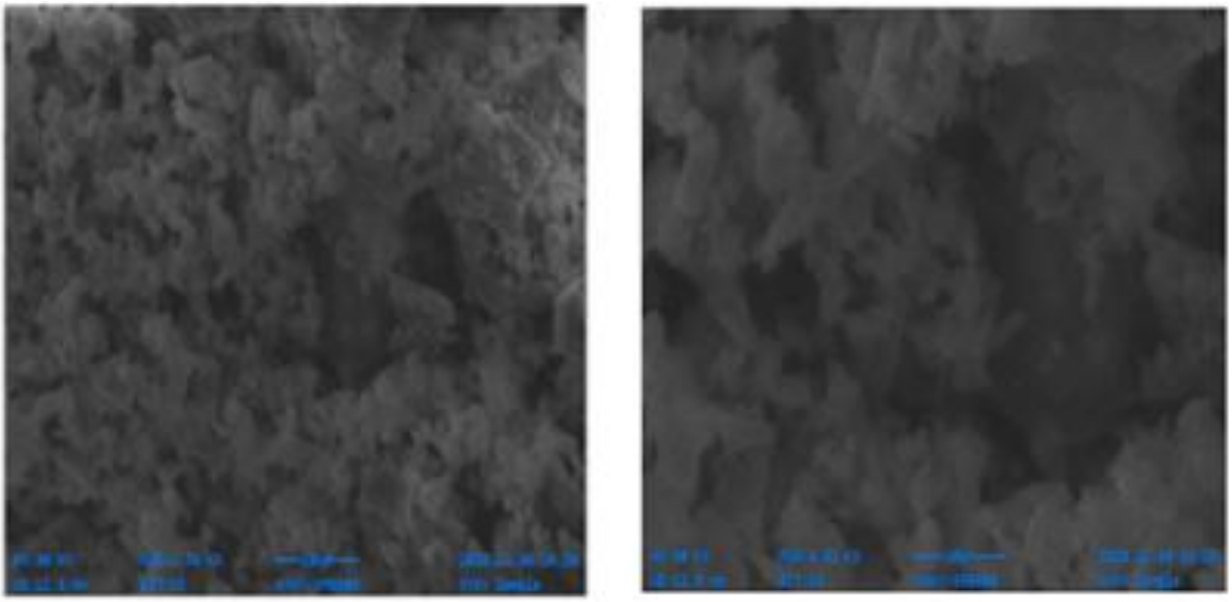

Figure 7. shows the SEM images of WSe2 nanosheet with different resolutions.

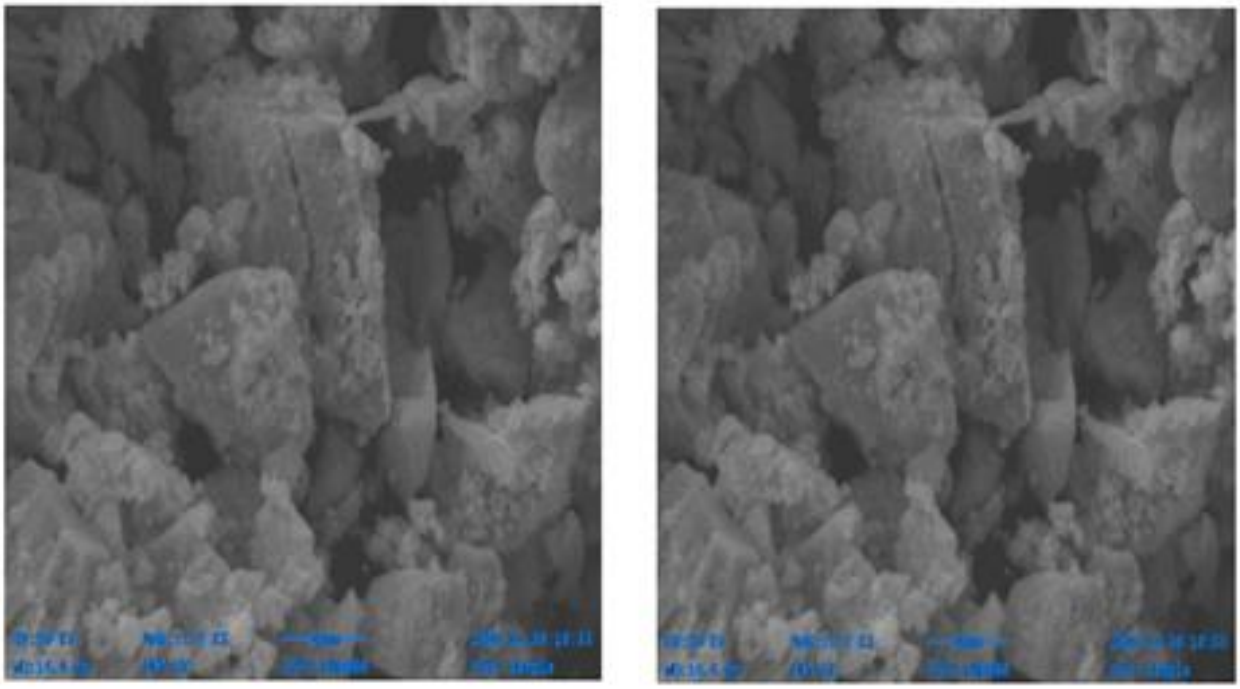

Figure 8. Shows the SEM images of WSe2 nanosheet with different resolutions.

Conclusion

This work utilized the hydrothermal approach to effectively produce and analyze WSe_2 nanosheets. While FTIR analysis validated the material's chemical composition and purity, SEM revealed the consistent shape and nanoscale size of the nanosheets. These results pave the way for further investigation into the electrical and optical properties of WSe_2 nanosheets, suggesting that they hold significant potential for use in optoelectronic devices.

References:

1. Wang, H., Yuan, H., Hong, S. S., Li, Y., & Cui, Y. (2015). Physical and chemical tuning of two-dimensional transition metal

dichalcogenides. Chemical Society Reviews, 44(9), 2664-2680.

2. Kumar, V. P., & Panda, D. K. (2024). 2D Material Tungsten Diselenide (WSe_2): Its Properties, Applications, and Challenges. Nanoelectronic Devices and Applications, 271-296.

3. Cheng, Q., Pang, J., Sun, D., Wang, J., Zhang, S., Liu, F., ... & Zhou, W. (2020). WSe_2 2D p-type semiconductor-based electronic devices for information technology: design, preparation, and applications. InfoMat, 2(4), 656-697.

4. Joseph, S., Mohan, J., Lakshmy, S., Thomas, S., Chakraborty, B., Thomas, S., & Kalarikkal, N. (2023). A review of the synthesis, properties, and applications of 2D transition metal dichalcogenides and their heterostructures. Materials Chemistry and Physics, 297, 127332.

5. Tao, L., Chen, Z., Li, Z., Wang, J., Xu, X., & Xu, J. B. (2021). Enhancing light-matter interaction in 2D materials by optical micro/nano architectures for high-performance optoelectronic devices. InfoMat, 3(1), 36-60.

6. Cheng, Q., Pang, J., Sun, D., Wang, J., Zhang, S., Liu, F., ... & Zhou, W. (2020). WSe_2 2D p-type semiconductor-based electronic devices for information technology: design, preparation, and applications. InfoMat, 2(4), 656-697.

7. Ndlwana, L., Raleie, N., Dimpe, K. M., Ogutu, H. F., Oseghe, E. O., Motsa, M. M., ... & Mamba, B. B. (2021). Sustainable hydrothermal and solvothermal synthesis of advanced carbon materials in multidimensional applications: A review. Materials, 14(17), 5094.

8. Azam, A., Yang, J., Li, W., Huang, J. K., & Li, S. (2023). Tungsten diselenides (WSe2) quantum dots: Fundamental, properties, synthesis and applications. Progress in Materials Science, 132, 101042.

9. Rastikian, J. (2021). Experimental investigation of charge and spin transport in WSe_2 connected with palladium contacts (Doctoral dissertation, Université Paris Cité).

10. Alzaid, M., Hadia, N. M. A., Shaaban, E. R., El-Hagary, M., & Mohamed, W. S. (2022). Thickness controlling bandgap energy, refractive index and electrical conduction mechanism of 2D Tungsten Diselenide (WSe_2) thin films for photovoltaic applications. Applied Physics A, 128(2), 94.

11. Azam, A., Yang, J., Li, W., Huang, J. K., & Li, S. (2023). Tungsten diselenides (WSe_2) quantum dots: Fundamental, properties, synthesis and applications. Progress in Materials Science, 132, 101042.